Experimental Investigation on the Reflectivity of Al, Cu, Zn and Ni and its Comparison with Theory

Jack Jinn-goe Hsia

DISCLAIMER NOTICE

THIS DOCUMENT IS BEST QUALITY PRACTICABLE. THE COPY FURNISHED TO DTIC CONTAINED A SIGNIFICANT NUMBER OF PAGES WHICH DO NOT REPRODUCE LEGIBLY.

EXPERIMENTAL INVESTIGATION ON THE REFLECTIVITY OF Al, Cu, Zn AND Ni AND ITS COMPARISON WITH THEORY

Contract. N00014-67-A-0226-0002.

A Thesis

Submitted to the Faculty

of

Purdue University

by

Jack Jinn-goe Hsia

In Partial Fulfillment of the

Requirements for the Degree

of

Doctor of Philosophy

August 1968

ACKNOWLEDGEMENT

Appreciation is hereby extended to the author's joint major professors, Dr. Y. S. Touloukian and Dr. D. P. DeWitt, for their invaluable critical evaluation of this study, and still more, for their constant advice and encouragement during the entire period of the author's graduate study.

The author wishes to acknowledge with gratitude the financial assistance provided by the Office of Naval Research, Physics Branch, which made this work possible.

TABLE OF CONTENTS

LIST OF TABLES

LIST OF FIGURES

NOMENCLATURE

Latin Letters

Symbol	Definition
a	The spherical area of entrance port (flux averaging sphere)
A	Absorptivity
A_o	Absorptivity with diffuse scattering electrons.
A_1	Absorptivity with specular scattering electrons.
A_B	Bulk absorptivity.
b	Effective prism base. Also spherical area of detector port (flux averaging sphere).
b_{ep}	Quantum correction factor due to electron-phonon interaction.
b^o_{ep}	dc value of quantum correction factor due to electron-phonon interaction.
B_D	Total flux reaching the detector port of the flux averaging sphere.
c	Speed of light. Also spherical area of sample port (flux averaging sphere).
D	Diameter of paraboloid mirror in the monochromator.
D_1	Recorder deflection corresponding to SPECIMEN IN position.
D_2	Recorder deflection corresponding to SPECIMEN OUT position.
e	Charge of an electron.
$\bar{E}$	Electric field.
E_λ	The power emitted by the source per unit area per unit solid angle per unit wavelength.

Symbol	Definition
$E_\lambda \Delta\lambda$	The power emitted by the source per unit area per unit solid angle in the $\Delta\lambda$ range.
f	Electron distribution function. Also, focal length.
$\hbar$	Planck's constant/2 π.
$\overline{H}$	Magnetic field
I'	Intensity after one reflection.
I"	Intensity after three reflections.
$\overline{J}$	Current density.
k	Absorption coefficient.
K	Boltzmann constant
ℓ	Height of the slit.
m	Mass of an electron.
n	Index of refraction.
n*	Complex index of refraction.
N	The number of electrons per unit volume.
p	Fraction of electrons which are reflected specularly.
P	Total radiant flux incident into the incident port of the flux averaging sphere.
R	Reflectivity. Also, radius of the sphere.
R_i	Reflectivity in each of the four orientations.
ΔR	Uncertainty of reflectivity.
r'	Reflectivity of standard mirror.
r	Surface resistance.
r_s	Reflectance of the Sample.
r_w	Reflectance of sphere wall.
S	Poynting vector.

Symbol	Definition
s	Mechanical slit width.
T	Temperature.
ΔT	Uncertainty of transmission.
$\overline{W}$	Power expenditure.
v	Electron velocity.
v_f	Fermi velocity.
x	Surface reactance.
Δx	Slit width.
z	Penetration distance of the wave.
Z	Impedance of surface.

Greek Letters

α	Prism apex angle. Also polarizability.
γ	Damping coefficient.
γ_{ee}	Damping coefficient due to electron-electron interaction.
γ_{ep}	Damping coefficient due to electron-phonon interaction.
γ^o_{ep}	dc value of damping coefficient due to electron-phonon interaction.
ϵ	Real dielectric constant.
$\overline{\epsilon}$	Complex dielectric constant.
δ	Depth of penetration.
δ_s	Skin depth.
θ	Angle.
θ_D	Debye temperature.
λ	Wavelength (in microns).

Symbol	Definition
$\Delta\lambda$	Spectral slit width.
$(\Delta\lambda)_d$	Spectral slit width due to dispersion of the prism.
$(\Delta\lambda)_p$	Spectral slit width due to Rayleign diffraction.
ρ	Electrical resistivity (in ohm-cm).
σ	Electrical conductivity (in cgs esu unit).
$\overline{\sigma}$	Dimensionless conductivity defined by Equation(41).
σ_o	Direct current conductivity.
η	Efficiency of the sphere.
τ	Relaxation time.
μ	Permeability.
ν	Frequency.
$\overline{\nu}$	Dimensionless frequency defined by Equation (42).
ω	Angular frequency.
ω_o	Plasma frequency.
Ω_{ee}	Defined by Equation (56).

ABSTRACT

Hsia, Jack Jinn-Goe, Ph. D., Purdue University, August 1968. Experimental Investigation on the Reflectivity of Al, Cu, Zn, and Ni and Its Comparison with Theory. Joint Major Professors: Yeram S. Touloukian and D. P. DeWitt.

This study is to generate accurate experimental results on reflectivity of metals and to compare them with the predictions made by theoretical models and also to predict values in longer wavelength range not covered by this experiment.

The theories of the reflectivity of metals are first reviewed with respect to macroscopic and microscopic points of view. Apparatus was built for measuring normal spectral reflectivity by using a multiple reflection technique. Measurements of normal spectral reflectivity were made on the bulk surface of the pure metallic elements, copper, zinc, and nickel and high vacuum evaporated surface of pure aluminum. The measurements were made from 2 to 13μ in air, at room temperature.

The absorptivity predicted by the theory of anomalous skin effect assuming diffuse electronic reflection, one electron per atom, and bulk conductivity, is found to have lower values than those obtained in the present experiment. On the other hand, the prediction which is made by the

simple equation derived from quantum theory is found to fit well with the experimental results.

Simple Drude Theory and Hagen-Rubens relation are used to predict absorptivity values in the longer wavelength range not measured in this experiment. Most probable absorptivity values of copper, zinc, nickel, and aluminum from two to one hundred microns are obtained based on measurement and theory.

I. INTRODUCTION

Attainment of better understanding of the fundamental processes involved in the interaction of electromagnetic radiation is intrinsically desirable; further, it can contribute to achieving the following four immediate objectives. First, a detailed knowledge of the mechanism of the interaction of electromagnetic fields with matter allows determination of the detailed internal structure of materials and thereby a more complete knowledge of their physical properties. Second, if the thermal radiation properties can be related to other more easily evaluated properties of materials, the measurement will be simplified. Third, if meaningful and practical equations can be found or derived to predict thermal radiation property data, obtained at a relatively few temperatures and wavelengths, over much wider temperature and wavelength ranges, the advantage is that laborious and expensive measurement programs can be substantially reduced. Fourth, such a knowledge can help in the development and evaluation of equipment and techniques for measuring the thermal radiation properties of materials.

The first logical step is to investigate the ideal pure metallic elements. Ideal materials do not need

characterization in contrast to materials being used in practical engineering environments. It is extremely difficult to identify the surface characteristics. Although ideal materials are not of prime interest for technological applications, it must be appreciated that before real metallics or alloys can be rationally studied and characterized, it is essential to thoroughly understand the ideal metals. This study also complements present activities at TPRC and in particular will provide critical information in support of an analysis type program to establish standard reference data for the metallic elements.

Classical optics of metals has been well reviewed (12)*, and the interrelations of properties summarized. A significant feature of solid-state physics during the last two decades has been the development of the theory of the anomalous skin effect in metals. This discovery has led to a revolution in ideas about the physical properties of metals, including their optical properties at low temperatures. Quantum theory of optical phenomena in metals reveals much valuable information about their internal structure.

The range from one or two microns to longer wavelengths is the controlling region for the heat transfer parameters. At 450°C only 1% of the radiant energy falls below two microns and at 2000°C only about 10%. The total radiation

---

*Numbers in parenthesis refer to the "List of References."

properties are of prime interest to the engineers. These can be easily obtained by simply integrating the spectral properties over the wavelengths. The modern technical trend is toward studies at low temperatures and at low temperature the long wavelength radiation properties are of more practical usage. As the first experimental phase of a long range program at the Thermophysical Properties Research Center on the determination of thermal radiation properties, an apparatus capable of yielding high accuracy results has been extensively evaluated and explored. High accuracy of the apparatus is required for obtaining precise data for the assessment of both the theoretical predictions at room temperature in the present study and the comparison of results at different temperatures for other phases of the program in the future. In the present study, a multiple reflection technique is used. It lends itself to high accuracy experimental measurements. With the instrumentation available, normal spectral properties in the wavelength range of two to 13 microns are chosen for this study. This is the wavelength range of normal dispersion where simple theoretical equations are available.

II. THEORIES ON REFLECTIVITY OF METALS

A. Macroscopic Theory

The propagation of electromagnetic waves within a homogeneous, isotropic medium having a conductivity characteristic of a metallic conductor can be treated on the basis of the phenomenological theory of classical electrodynamics (42).

The Maxwell's field equations are expressed as

$$\text{Curl } \bar{H} = \frac{\epsilon}{c} \frac{\partial \bar{E}}{\partial t} + \frac{4\pi\sigma}{c} \bar{E} \qquad 1$$

$$\text{Curl } \bar{E} = -\frac{\mu}{c} \frac{\partial \bar{H}}{\partial t} \qquad 2$$

$$\text{div } \bar{H} = 0 \qquad 3$$

$$\text{div } \bar{E} = 0 \qquad 4$$

where $\bar{H}$ is the magnetic field, $\bar{E}$ is the electric field, ϵ is the dielectric constant, σ is the electrical conductivity, and μ is the permeability which is very close to unity for paramagnetic and diamagnetic materials (42).

Upon solving the field equations, Equations 1 to 4, the electrical field can be expressed as

$$\bar{E} = \bar{E}_0 \exp \left\{ i \left[\frac{\omega}{c} \left(\epsilon + \frac{4\pi\sigma i}{\omega} \right)^{\frac{1}{2}} z - \omega t \right] \right\} \qquad 5$$

where ω is the angular frequency and z is the penetration distance of the wave.

The complex index of refraction n* is defined as

$$n^* = (n - ik) = \left(\epsilon + \frac{4\pi\sigma i}{\omega}\right)^{\frac{1}{2}} \qquad 6$$

where n is the index of refraction and k is the index of absorption. Thus Equation 5 can be written as

$$\overline{E} = \overline{E}_0 \exp\left\{i\omega\left(\frac{z}{c/n} - t\right)\right\} \exp\left(-\frac{k\omega z}{c}\right) \qquad 7$$

the phase velocity is reduced to c/n, (from the first exponential term) and the wave is damped (from the second exponential term) as it propagates, by a fraction exp (- $2\pi k$) per wavelength.

Equation 6 yields the important relations between the electrical properties (ϵ,σ) and optical constants (n,k):

$$\epsilon = n^2 - k^2 \qquad 8$$

$$\sigma = nk\omega/2\pi \qquad 9$$

The reflectivity, R, of a metal is defined as the ratio of the radiant flux of the reflected and incident waves. The radiant flux of the wave is proportional to the square of the modulus of the electric field amplitude. The Fresnel relation derived from Maxwell equations satisfying continuity conditions of the electromagnetic fields gives the well-known result that for normal incidence (21)

$$R = \left|\frac{n^* - 1}{n^* + 1}\right|^2 \qquad 10$$

or

$$R = \frac{(n-1)^2 + k^2}{(n+1)^2 + k^2} \qquad 11$$

The normal absorptivity of an opaque substance is related to the normal reflectivity by the relation

$$R = 1 - A \qquad 12$$

and by Equation 11, the absorptivity is related to the optical constants

$$A = \frac{4n}{(n+1)^2 + k^2} \qquad 13$$

For long wavelengths (approximately λ>100 microns) $(\sigma/\nu) >> \epsilon$, where ν is $\omega/2\pi$. Equations 8 and 9 yields

$$n = k \approx (\sigma/\nu)^{\frac{1}{2}} \qquad 14$$

Neglecting the higher order terms, the reflectivity of a metal from Equation 11 simplified to

$$R \approx 1 - \frac{2}{n} \qquad 15$$

which leads to the following well-known Hagen-Rubens equation (neglecting the higher order terms)

$$R = 1-2\ (\nu/\sigma)^{\frac{1}{2}} \qquad 16$$

where σ is in cgs esu units. Equation 16 will be in the form of

$$R = 1 - 36,5\ (\rho/\lambda)^{\frac{1}{2}} \qquad 17$$

if ρ is in ohm-cm, and λ in microns.

As a result of the electrical field within the metal, a current flow occurs. The current per unit area is called current density and the total current density $\bar{J}$ can be defined

(51) as

$$J = \frac{c}{4\pi} \text{curl } \overline{H} \qquad 18$$

Upon inserting Equation 1 into Equation 18 and replacing the dielectric constant ϵ with $1+4\pi\alpha$ where α is the polarizability, Equation 18 becomes

$$\overline{J} = \frac{1}{4\pi} \frac{\partial \overline{E}}{\partial t} + \alpha \frac{\partial \overline{E}}{\partial t} + \sigma \overline{E} \qquad 19$$

where α and σ are real. From Equation 19, it follows that the total current density consists of three components; namely, the pure displacement current (first term), the polarization current, and the conduction current. The conduction current constitutes the motion of free charges; the polarization current is associated with bound charges. Since the pure displacement current is not accompanied by motion of charges, the current density may thus be defined as

$$\overline{J} = \alpha \frac{\partial \overline{E}}{\partial t} + \sigma \overline{E} \qquad 20$$

or

$$\overline{J} = (\sigma + i\omega \alpha)\overline{E} \qquad 21$$

It should also be noted that the phase difference between the polarization current and $\overline{E}$ is 90°, so that this current does not dissipate the energy of the field; the conduction current is always in phase with the electric field and therefore continuously dissipates the energy of the field. Hence, the absorption of electromagnetic waves by a medium is proportional with σ as commonly expressed by Ohm's Law

$$\overline{J} = \sigma \overline{E} \qquad 22$$

In the classical theory it is assumed that the current density at a given point is unambiguously defined when the field strength at a point is given. A further assumption is made that the electric field may be looked upon as uniform when the current density is calculated. This is not valid when the "anomalous skin effect" is considered as will be discussed later.

B. Microscopic Theory

1. Classical Considerations - Simple Free Electron Model

The classical theory of reflectivity or absorptivity of metals based on the free electron model was developed by Drude and Zener*.

Drude was the first to suggest that the fundamental physical properties of metals can be explained by assuming the existence of a free electron gas moving between the ions which form the crystal lattice of the metal. These electrons are in thermal equilibrium with the ions. When a constant electric field is applied to the metal, the electrons are accelerated in the direction of the field. Therefore, the random motion of the electrons is augmented by the directed acceleration, which is responsible for the appearance of the electric current. If there were no collisions between the electrons and the lattice, the energy communicated to the electrons by the field would increase indefinitely,

*See for example in references 12 and 51.

resulting in an infinite mean free path, the mean distance travelled by electrons between collisions. This would lead to zero electrical resistivity. The fact that metals have a finite resistivity suggests that collisions between electrons and lattice ions do occur.

When the damping due to the resistance of the metal is considered, the equation of motion for a free electron is

$$m\ddot{r} + m\gamma\dot{r} = e\bar{E} \qquad 23$$

where γ is the damping coefficient, r is the electron position coordinate within the metal, $\bar{E} = \bar{E}_o e^{-i\omega t}$ is the applied electromagnetic field, and e and m are the charge and mass of an electron.

Upon solving the equation of motion (Equation 23) for the velocity $\dot{r}$, the current density $\bar{J}$ is obtained by using the relation $\bar{J} = Ne\dot{r}$. The electrical properties (σ,ϵ) are obtained from the relation between the current density and electric field (Equation 21). Equations 8 and 9 for the relations between the electrical properties (σ,ϵ) and optical constants (n,k) then give the Drude-Zener formulas:

$$n^2-k^2 = 1 - \frac{4\pi Ne^2}{m} \frac{1}{\omega^2+\gamma^2} \qquad 24$$

$$nk = \frac{2\pi Ne^2}{m\omega} \frac{\gamma}{\omega^2+\gamma^2} \qquad 25$$

where N is the number of electrons per unit volume. The coefficient γ is related to the dc electrical conductivity by the relation

$$\gamma = \frac{Ne^2}{m\sigma_o} \qquad 26$$

The normal spectral reflectivity or absorptivity can be expressed in terms of N, e, m, γ by means of Eauations 11, 13, 24, and 25.

The results of the Drude-Zener theory when compared with experimental measurements show fair agreement for the liquid metals Hg and Ga (31), and ultra-high vacuum deposited silver gold, and aluminum (4). In general, the theory fails in the higher frequency region of the spectrum and also at low temperatures.

2. Multi-free/bound Electron Theory

Roberts has suggested (44,45,46) and the quantum theory has also exposed the idea, that a real metal consists of several types of free and bound electrons existing in a metal, and both types of electrons exist in different energy states (12). As such, they react in different degrees to the influence of an electric field induced by the incident radiation. The free electrons of a particular type are distinguished by the damping coefficient as previously suggested. The bound electrons influenced by the induced electric field can be assumed to be characterized by an elastic restoring force and a viscous damping force. Equations of optical properties and radiative properties can be derived by starting with the equations of motion for different types of electrons using the procedure discussed in the previous

section. The resulting equations are rather complicated and involve parameters mentioned above as well as the number density of the different types of electrons.

Roberts has tested this model for several metals and evaluated the constants required from measurements of the optical constants. In each case of the metal observed, it was possible to determine values of a finite number of the constants which gave an acceptable comparison between data and theory. Attempts were made by Richmond, et al.(43) to determine the values of the parameters which would fit the normal spectral reflectivity spectrum of rhodium by using the multi-free/bound electron model. The comparison of the theory and data was very favorable. However, the optical constants computed from the parameters in the visible portion of the spectrum (where the computed curve shows good agreement with experimental data) did not agree with measured optical constants for the same wavelengths. Hence, it is evident that this model suffers from its cumbersome form and large number of parameters, giving an appearance of mathematical expediency rather than physical reality. Additional tests of this model require optical constants data or complete reflectivity spectra. For testing this model in the infrared range the parameters for the bound electrons can be dropped because they are not important in this wavelength range.

3. The Anomalous Skin Effect

a. Basic Concept. As the temperature is lowered, the depth of penetration*, δ, of the high frequency field into the metal decreases as a result of the increase in electrical conductivity; the mean free path increases and may become comparable with or much greater than the depth of penetration. In this condition the electrons will succeed in traversing regions with different field strength in one mean free path, and the additional velocities which they will acquire as a result of this process will depend on the field strength along the entire path. This means that Ohm's Law $\bar{J} = \sigma\bar{E}$ in which σ is constant for all parts of the metal, must be replaced by a more general equation in which $\bar{J}$ should be a function of field strength and position. This is the anomalous skin effect in which the expression of the electric field strength is given by a very complicated form, derived from the electron distribution function and Maxwell field equations, and is not exponential in form as in the case of classical theory (refer to Equation 7). As long as the propagation of the wave is no longer exponential in nature, the classical representation involving the complex refractive index, defined from the exponential form of the electric

*Referring to Equation 7, the depth of penetration, defined as the distance traversed by the wave within the material where the wave amplitude is reduced by a factor of 1/e, can be expressed as $\delta = \lambda/2\pi k$. At long wavelengths, $k = (\sigma_0/\nu)^{\frac{1}{2}}$, therefore $\delta = c/(2\pi\omega\,\sigma_0)^{\frac{1}{2}}$. This is not to be confused with the skin depth, $\delta_s = (mc^2/4\pi Ne^2)^{\frac{1}{2}}$, which is the distance of one wavelength corresponding to the plasma frequency.

field, is no longer physically significant. The more general term "surface impedance" Z is introduced and defined as the ratio of the electric field at the surface of the metal to the total current per unit area. By using Maxwell's field equations, the surface impedance Z can be expressed as

$$Z = -\frac{4\pi i\omega}{c^2} (E)_{z=0} \Big/ \left(\frac{\partial E}{\partial z}\right)_{z=0} \qquad 27$$

or

$$Z = 4\pi c \ (E)_{z=0} / (H)_{z=0} \qquad 28$$

At normal incidence the absorptivity in terms of the impedance concept is given by

$$R = 1 - A = \left|\frac{4\pi/c - Z}{4\pi/c + Z}\right|^2 \qquad 29$$

where, $4\pi/c$ and Z are the impedance of free space and metal surface respectively. Equation 29 can also be written as

$$R = 1 - A = \left|\frac{\frac{4\pi}{c}\frac{1}{Z} - 1}{\frac{4\pi}{c}\frac{1}{Z} + 1}\right|^2 \qquad 30$$

Comparison between Equations 30 and 10 reveals the relationship between the surface impedance and complex index of refraction as

$$n^* = \frac{4\pi}{c}\frac{1}{Z} \qquad 31$$

Furthermore, when the surface impedance Z is expressed as $r + ix$, where r is the surface resistance and x is the surface reactance, expanding Equation 29 in series yields

$$A = \frac{cr}{\pi}\left\{1 - \frac{1}{16}\left(\frac{cx}{\pi}\right)^2 \cdots\right\} - \frac{1}{2}\left(\frac{cr}{\pi}\right)^2 \qquad 32$$

The second and higher powers of x may be neglected. This is tantamount to neglecting the displacement current, the photoelectric current[‡], and the atomic polarizability since these currents are not dissipating the energy of the electric field just as the condition of the surface reactance x. The term r^2 can also be neglected if the absorbing power is small, a fact which is valid for good conductors. Thus the following final expression for the absorptivity is obtained.

$$A = \frac{cr}{\pi} \qquad 33$$

The microscopic phenomena of metals upon receiving an electromagnetic wave may be discussed as follows. The conduction electrons in the metal interact with the lattice and with each other. An electromagnetic wave is incident on the surface of the metal. The electron energy distribution (Equilibrium Fermi distribution) is modified under the action of the electromagnetic field and as a result of collisions between electrons and between electrons and the lattice. If the change in the equilibrium function is small, the perturbation theory can be used to obtain the electron distribution function, f, then the current density can be calculated by using the following Equation (37).

$$J(z) = -2e \left(\frac{m}{h}\right)^3 \iiint v_x f dv_x dv_y dv_z \qquad 34$$

The electric field strength can be obtained by using the following equation derived from the Maxwell's field equations.

[‡]The photoelectric current is due to the flow of electrons emitted from the surface as a result of the interaction between the conduction electrons and the electromagnetic field.

$$\frac{d^2E}{dz^2} + \frac{\omega^2}{c^2}E = \frac{4\pi i\omega}{c^2} J \qquad 35$$

Once the expression of the electric field strength is derived, the surface impedance Z can be obtained by using Equation 27.

b. Normal Skin Effect. The theory of normal skin effect (which is identical to the classical theory discussed in the previous section as will be seen in the following development) differs from the theory of the anomalous skin effect. In the former theory the change of the electron distribution function in the penetration direction is neglected, a fact which is valid when the mean free path is much smaller than the depth of penetration. The electric field strength thus derived is exponential in form and the surface impedance is given as

$$Z = \frac{4\pi\omega}{c^2}\left[\frac{\omega^2}{c^2} - \frac{4\pi i\omega\sigma}{c^2(1+i\omega\tau)}\right]^{-\frac{1}{2}} \qquad 36$$

where τ is the relaxation time which is equal to γ^{-1}. Using the relation between the surface impedance and complex index of refraction as stated in Equation 31, Equation 36 has the same form as the Drude-Zener formulas (i.e., Equations 24 and 25 when Ne^2/m is replaced by $\gamma\sigma$ as stated in Equation 26).

At surficiently long wavelengths ($\omega\tau<<1$) the free electrons dominate, thus the displacement can be neglected since it is not associated with charges. Equation 36 becomes

$$Z = r + ix = \sqrt{\frac{2\pi\omega}{c^2\sigma}}\,(1+i) \qquad 37$$

From Equation 37 the surface resistance is expressed as

$$r = \left(\frac{2\pi\omega}{c^2\sigma}\right)^{\frac{1}{2}} \qquad 38$$

c. Anomalous Skin Effect. When the mean free path is comparable with or much greater than the depth of penetration, the change of the electron distribution function in the penetration direction can no longer be neglected. With the above consideration Reuter and Sondheimer* developed the quantitative theory of the anomalous skin effect. Dingle (14) simplified their expressions in the visible and infrared region ($0.1<\lambda<30$ microns) and gave the expressions of absorptivity for the following two special cases: (1) perfectly specular reflection of electrons at the inner surface of the metal ($p = 1$) and (2) perfectly diffuse reflection ($p = 0$), namely,

$$A_{p=1} = \frac{v_f}{c}\left[\sqrt{3\bar{\sigma}}^{-1} + \bar{\nu}^{-2}\left(\frac{2}{3} + \frac{2}{\sqrt{3}}\bar{\sigma}^{-1} - \frac{\sqrt{3}}{8}\bar{\sigma}^{-3}\right)\right] \qquad 39$$

and

$$A_{p=0} = \frac{v_f}{c}\left\{\sqrt{3}\left(\frac{\sqrt{3}}{4} + \bar{\sigma}^{-1}\right) - \bar{\nu}^{-2}\left[\left(\frac{16\ell n2}{105} + \frac{8723}{80640}\right) + \frac{83\sqrt{3}}{192}\bar{\sigma}^{-1} + \frac{3}{4}\bar{\sigma}^{-2} + \frac{\sqrt{3}}{8}\bar{\sigma}^{-3}\right]\right\} \qquad 40$$

where v_f is the Fermi velocity and $\bar{\sigma}$ and $\bar{\nu}$ are the dimensionless conductivity and frequency, respectively, given by

---

*See for example in reference 51.

$$\bar{\sigma} = \sigma\left[\frac{v_f}{c}\left(\frac{3\pi m}{Ne^2}\right)^{\frac{1}{2}}\right] \qquad 41$$

and

$$\bar{\nu} = \nu\left[\frac{2}{3}\frac{c}{v_f}\left(\frac{3\pi m}{Ne^2}\right)^{\frac{1}{2}}\right] \qquad 42$$

Holstein (31), using energy balance considerations, derived the absorptivity expression for the case when the mean free path approaches infinity, i.e., at very low temperature

$$A = p\,\frac{2\pi Ne^2 v_f^3}{m\,\omega^2 c^3} + (1 - p)\,\frac{3v_f}{4c} \qquad 43$$

where p is the fraction of electrons which are reflected specularly. Thus, for the case of diffuse reflection of electrons

$$A_0 = \frac{3}{4}\frac{v_f}{c} \qquad 44$$

And for the case of specular reflection

$$A_1 = \frac{2\pi Ne^2 v_f^3}{m\omega^2 c^3} \qquad 45$$

Expressed in terms of the dimensionless frequency as stated in Equation 42, A_1 can be written as

$$A_1 = \frac{2}{3}\frac{v_f}{c}\,\bar{\nu}^{-2} \qquad 46$$

Equation 46 can also be obtained from Equation 40 when allowing $\bar{\sigma}$ to approach ∞, as is the case for very low temperatures.

4. Quantum Theory

From Equations 9 and 25 of the classical theory, the conductivity can be expressed as

$$\sigma = \frac{Ne^2}{m} \frac{\gamma}{\omega^2 + \gamma^2} \qquad 47$$

or

$$\sigma = \frac{\omega_0^2}{4\pi} \frac{\gamma}{\omega^2 + \gamma^2} \qquad 48$$

where $\omega_0 = (4\pi Ne^2/m)^{\frac{1}{2}}$ is the frequency characteristic of the electron plasma oscillation. The plasma frequency is generally outside the high-frequency limit of the free-electron dispersion spectrum. For example, the plasma frequencies of silver, gold, copper, and aluminum are 0.31, 0.50, 0.575, and 0.8 micron, respectively (34,37).

Holstein (31) used the perturbation theory to obtain the damping coefficient γ. With γ known as a function of wavelength and temperature, the conductivity σ can be calculated by using Equation 48. The dielectric constant ϵ should be obtained from the Kramers-Kronig relation

$$\frac{1 - \epsilon}{4\pi} = \frac{2}{\pi} \int_0^\infty \frac{\sigma(\omega')d\omega'}{(\omega'^2 - \omega^2)} \qquad 49$$

since upon relating Equations 24 and 8, the expression for ϵ obtained in the form

$$\frac{1-\epsilon}{4\pi} = \frac{\omega_0^2}{4\pi} \frac{1}{\omega^2+\gamma^2} \qquad 50$$

which is inconsistent with the result when σ in the expression of Equation 47 is inserted in Equation 49. The reason

for such inconsistency is due to the fact that in quantum theory, the damping coefficient γ in the expression of σ (Equation 47) is a function of not only temperature but also wavelength. However, in the classical theory, γ is a function of temperature only. Therefore, Equations 49 and 50 can be used interchangeably in the classical theory. Once the electrical properties (σ, ϵ) are known, the optical constants (n,k) can be derived from Equation 8 and 9. Furthermore, the absorptivity is obtainable by using Equation 13 which relates the absorptivity and the optical constants. Some of the considerations that enter into the calculations are a. free electron theory, b. spherical Fermi surface, c. Fermi-Dirac Statistics of the electron distribution, d. Pauli exclusion Principle, and e. the classical treatment of electromagnetic field.

It is well-known that the power expenditure* $\overline{W}$ for a free electron system is related to the conductivity $\sigma(\omega)$ by the relation:

$$N\overline{W} = \frac{E^2}{2}\sigma(\omega) \qquad 51$$

where $\overline{W}$ is the power expenditure due to one electron per unit time and $E^2/2$ is the energy density per unit volume of the electromagnetic field.

---

*$\overline{W}$ is the time average of $-W = (\partial S_z/\partial z)$ where W is the Joule heat produced per unit time and per unit volume within the conducting medium, z is the distance of penetration and $\overline{S}$ is the Poynting vector which is defined as $\overline{S} = \frac{c}{4\pi}(\overline{E} \times \overline{H})$.

The power expenditure $\bar{W}$ is derived from the transition probability which is obtained by using the perturbation theory on solving the Schrödinger equation for a conduction electron interacting with the perturbing electromagnetic field and the lattice vibration.

The damping coefficient γ_{ep} due to electron-phonon interaction is given as:

$$\gamma_{ep}(\mu,\alpha) = \gamma^0_{ep}(\alpha) b_{ep}(\mu,\alpha) \qquad 52$$

Here

$$\mu = \left(\frac{\hbar\omega}{KT}\right) \qquad \text{and} \qquad \alpha = \left(\frac{\Theta_D}{T}\right)$$

where $\hbar$ is Planck's constant/2π, K is Boltzmann constant, Θ_D is the Debye temperature, and $b_{ep}(\mu,\alpha)$ is the quantum correction factor due to electron-phonon interaction.

The damping coefficient including the effect due to electron-electron interaction is given as

$$\gamma(\mu,\alpha) = \gamma^0_{ep}(\alpha) b_{ep}(\mu,\alpha) + \gamma_{ee}(\mu,\alpha) \qquad 53$$

where $\gamma_{ee}(\mu,\alpha)$ is the damping coefficient due to electron-electron interaction.

In the spectral region $\gamma^2 << \omega^2 << \omega_0^2$, Holstein obtained the following equations for optical constants (n,k):

$$n = \frac{1}{2}\frac{\omega_0}{\omega^2}\left(\gamma^0_{ep}(\alpha) b_{ep}(\alpha) + \frac{\omega^2}{\Omega_{ee}(\alpha)}\right) \qquad 54$$

$$k = \left(\frac{\omega_0}{\omega}\right) \qquad 55$$

In this region the quantum correction factor b_{ep} is

independent of wavelength and

$$\Omega_{ee}(\alpha) = \left(\frac{\hbar KT}{2\pi}\right)^2 \gamma^0_{ee}(\alpha) \qquad 56$$

Thus, the bulk absorptivity A_B can be expressed as

$$A_B = \frac{2}{\omega_0}\left(\gamma^0_{ep}(\alpha) b_{ep}(\alpha) + \frac{\omega^2}{\Omega_{ee}(\alpha)}\right) \qquad 57$$

Notice from Equation 54 that n is proportional to $(\lambda^2 + \text{constant})$ and k is proportional to λ for a fixed temperature. Thus, the plottings of n vs λ^2 and k vs λ will give ω_0, Ω_{ee} and $\gamma^0_{ep}(\alpha)$ since $b_{ep}(\alpha)$ is known from the theory. The quantity $\gamma^0_{ee}(\alpha)$ can be calculated by Equation 56. With all these parameters known, the bulk absorptivity can be easily obtained from Equation 57. Direct current conductivity can be calculated by using the equation

$$\sigma_0(\alpha) = \frac{\omega_0^2}{4\pi} \frac{1}{\gamma^0_{ep}(\alpha) + \gamma^0_{ee}(\alpha)} \qquad 58$$

III. METHODS OF NORMAL SPECTRAL REFLECTIVITY MEASUREMENTS

A. Calorimetric Method

The basic principle is to find the absorptivity by a comparison of the energy absorbed with the energy of the normally incident radiation in the absolute method or to find the absorptivity relative to a black surface in the comparative method.

1. Absolute Measurement

Biondi (7) used the calorimetric method to determine the absorptivities of copper and silver at 3.4 to 4.2°K over the wavelength range from 0.3 to 3.3 microns. The energy of the incident radiation absorbed on the surface of a metal specimen is determined by first measuring the rise in temperature of the specimen and then by turning off the incident radiation source and power being applied to the heater in the specimen stage (see Figure 1) to reproduce the temperature rise. The energy applied to the specimen heater is equivalent to the incident energy absorbed by the specimen. The total incident energy, the energy absorbed by the specimen plus the energy reflected by the specimen and absorbed by the black absorber, is

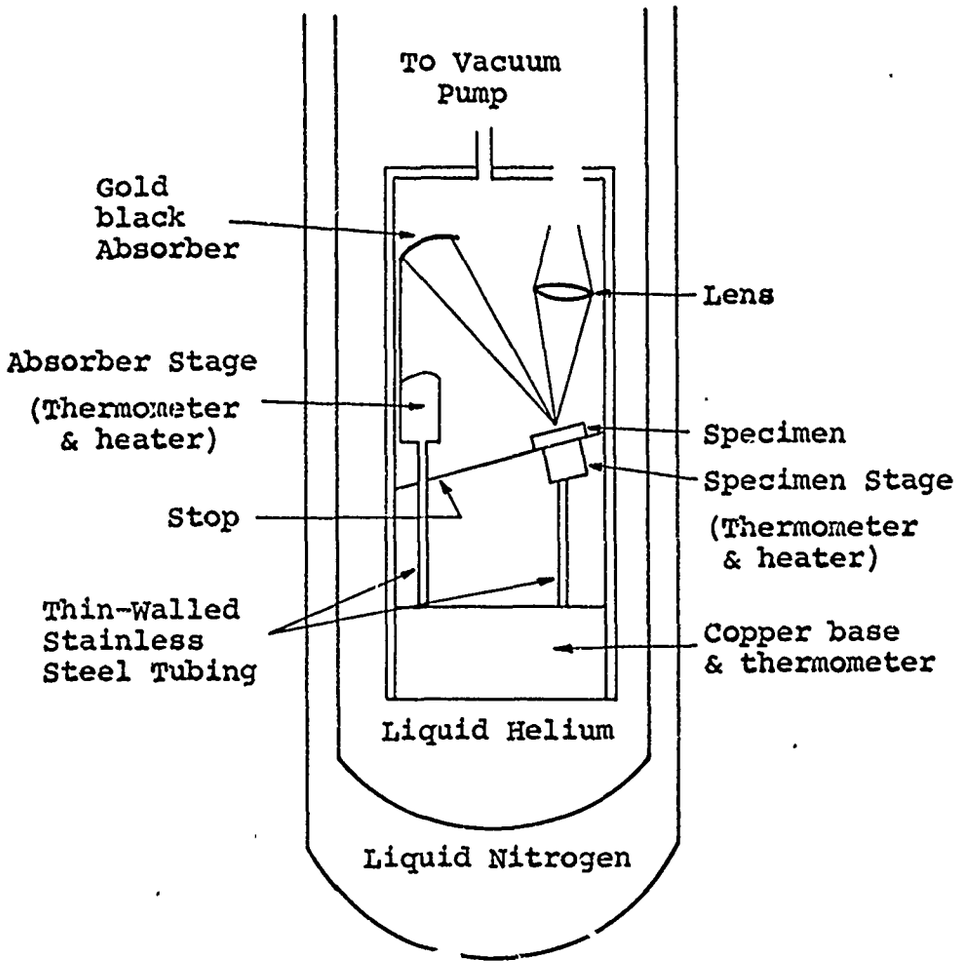

Figure 1. Schematic of Biondi's Apparatus.

equivalent to the energy required to put into the heaters in both the specimen stage and the absorber stage to reproduce the temperature rise. The temperature was determined by a carbon resistance thermometer. The precision was claimed around ±2%.

2. Comparative Measurement

Brandenberg, Clausen, and McKeown (8) measured the absorptivity of evaporated aluminum in the wavelength region from 0.45 to 2.0 microns by using a specimen which consists of a temperature-sensitive Y-cut quartz crystal plated on one side with the metal film to be studied and the other side with an opaque layer of benzene smoke, a highly absorbing coating. The small temperature rise of the plated crystal due to the energy absorbed from the incident beam of radiation is measured by monitoring the frequency change of the quartz crystal when it is used as an active element and driven in an oscillator. The absorptivity, relative to the black surface, is determined from frequency rates at a particular temperature as the crystal goes through a heating and cooling cycle. This method is claimed to give a possible precision in absorptance of ±1.4%. The schematic of the apparatus is shown in Figure 2.

The crystal holder is mounted rigidly to a metal hemisphere such that the center of the crystal coincides with the origin, and the black face is subtended by the hemisphere. This increases the blackness of the benzene smoke by

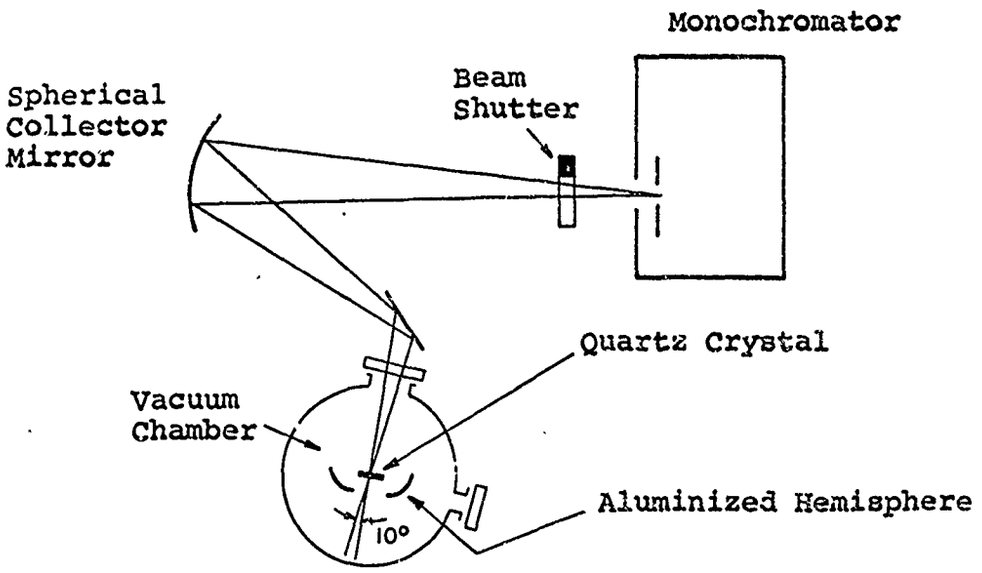

Figure 2. Schematic of the Apparatus Used by Brandenberg, et al.

refocusing reflected energy back onto the benzene surface. The crystal can be turned through 180° so that the beam is either incident on the sample electrode or incident through the hemisphere on the benzene smoke coating.

B. Single Reflection Method

Radiation energy received from a single reflection from the specimen is compared with the direct incident energy. Twidle's apparatus (53) illustrates this method (see Figure 3). The mirror (specimen) under investigation, M, could be swung into the beam so that, after reflection, the image of the slit S is formed on the thermopile T_2. Thus, this apparatus requires different detectors to measure the incident and reflected radiant flux. This will give rise to large errors in the measurement results.

C. Multiple Reflection Method (Strong's Method)

Multiple reflection techniques have been discussed by Strong (52) and Beattie (1). The basic principle of Strong's method can be illustrated by the original setup proposed by Strong (see Figure 4). The square of the absolute reflectance of the sample can be obtained from the ratio of two radiant flux readings corresponding to the two conditions shown in Figure 4. Because the square of the absolute reflectivity is measured, the value of the absolute reflectivity is obtained with higher precision than would be possible of there was only one reflection from the specimen.

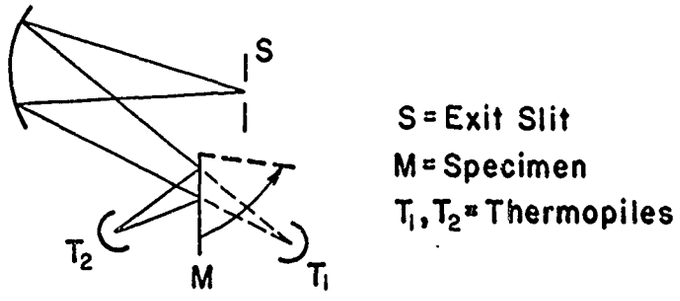

Figure 3. Schematic of Twidle's Apparatus.

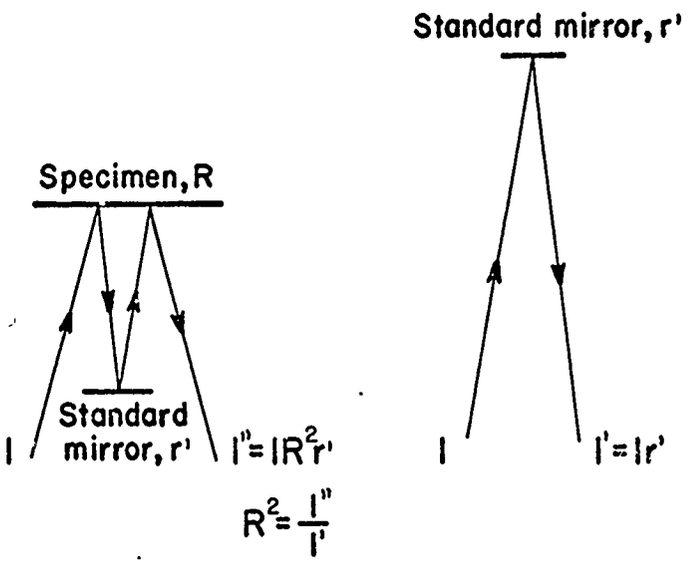

Figure 4. The Strong Technique.

1. Gates, Shaw, and Beaumont (22) Method

Gates et al., used the modified Strong's method by measuring the reflectivity of a matched pair of evaporated specimens, size three inches by ten inches. The flux of the radiation after being reflected from the parallel specimens 2,4, 6,8, and 10 times was recorded, and the reflectivity was determined as a root of the ratios of these readings. The incident angles were 20° to 60°, wavelength range 0.7 to 12 microns, and the specimens consisted of evaporated metal films. The accuracy of the measurement was said to be $\pm 0.2\%$. (Collimated radiation was used as the source.)

2. Fowler (Far Infrared) Method (20)

Fowler also used the modified Strong's method in the wavelength range 8.5 to 83.5 microns. The reflectivity was calculated from the ratio of the observed radiant flux after seven reflections to that observed after one reflection from the specimens. The incident angle was 23°, and the matched pairs of specimens were evaporated gold films on glass substrates. The specimen sizes were 7.6 cm X 3.8 cm and 4.8 cm X 3.8 cm. The accuracy stated was $\pm 0.2\%$.

3. Bennett (Visible, Averaging Sphere) Method(6)

Strong's method was used with both specimen and standard mirrors included. An averaging sphere was used to reduce the errors introduced by optics misalignment and spatial, angular, and area sensitivities of the detectors. Two block-type

specimen holders were used. Measurements were made with upper and lower blocks interchanged to eliminate the difference of the standard mirrors and also to reduce the geometrical defect of the blocks (e.g., being not exactly parallel). The angle of incidence is 7°, with two reflections on the specimen, and the accuracy is $\pm 0.1\%$.

4. Bennett (Visible and Infrared) Method (6)

About 1960, materials for the inner coating of the averaging sphere to be used in the near infrared range were not explored. Thus, Bennett developed an optical system with a unique compensating feature which prevented the image on the detector from changing size or position because of a slight tilt of the specimen. The angle of incidence is 5°, with two reflections from the specimen. The specimen size is 1.5-inch diameter disk. The accuracy is $\pm 0.1\%$.

5. Dunn (Infrared, Averaging Sphere) Method (17)

Dunn used averaging spheres to reduce the optical systematic errors. He used sulfur as the averaging sphere coating (18) which has a reflectance of approximately 0.95 to 0.75 for the wavelengths ranging from two to seven microns, respectively. The modified Strong's method was used to measure the reflectance of matched pairs of specimens with size of 0.5 inch X 0.25 inch. The optical path, when the specimens are in and out of the light path, were not identical. The incident angles were 0 to 52°, with one reflection of each

specimen of the matched pairs. The accuracy was given as ±0.15%.

D. General Comments

In the previous sections, various methods, such as the calorimetric method, single reflection method, and multiple reflection method, have been discussed.

Although the calorimetric method gives high accuracy in reflectivity (for low absorptivity materials), it is difficult to use the calorimetric methods in the infrared because of the low flux of the monochromator radiation available. The comparative measurement of calorimetric method appears capable of detecting very small temperature changes in the specimen only when the specimen is an evaporated film on Y-cut quartz crystal. Therefore, bulk specimens cannot be measured by using this method.

Single reflection method needs two detectors to receive incident and reflected radiation, and the accuracy of the measurement is poor. On the other hand, multiple reflection method generally yields more accurate results than the single reflection method. In the methods used by Gates et al., and Fowler, the radiant beam undergoes more than two reflections on the specimen surface, thus a relatively large size specimen is required which will increase the difficulty in preparing the bulk specimen. Also, in these apparatus because the incident angle has to be large, the measurement can no longer be considered as a normal reflectivity measurement (6).

Bennett's apparatus in both the visible and the infrared range and Dunn's apparatus in infrared range all employed special features to reduce the optical systematic errors.

IV. PRINCIPLE OF MEASUREMENT

An apparatus for measuring absolute normal spectral reflectivity is desired. Some special requirements are: the apparatus should be able to measure reflectivity in the infrared range from two to 13 microns, the apparatus should give accurate results ($\pm$0.002 reflectivity unit), the incident angle on the specimen should be less than 10°, the apparatus should be able to measure both thin film and bulk specimens, the specimen size required should be small (1x2 inches or 1-1¼ inch diameter) to simplify preparation of bulk specimens, and that optical systematic errors are kept as small as possible.

With these requirements in mind and from the comments of the previous section, the logical selection is an apparatus employing the multiple reflection method, an apparatus similar to that of Bennett's using two identical blocks as specimen holder and employing a flux averaging sphere with an inner coating usable in the infrared range.

Following is the principle of operation of the block type specimen holder. The measurements are made for four orientations of the specimen (see Figure 5) in order to reduce the effects of different reflectivities of standard

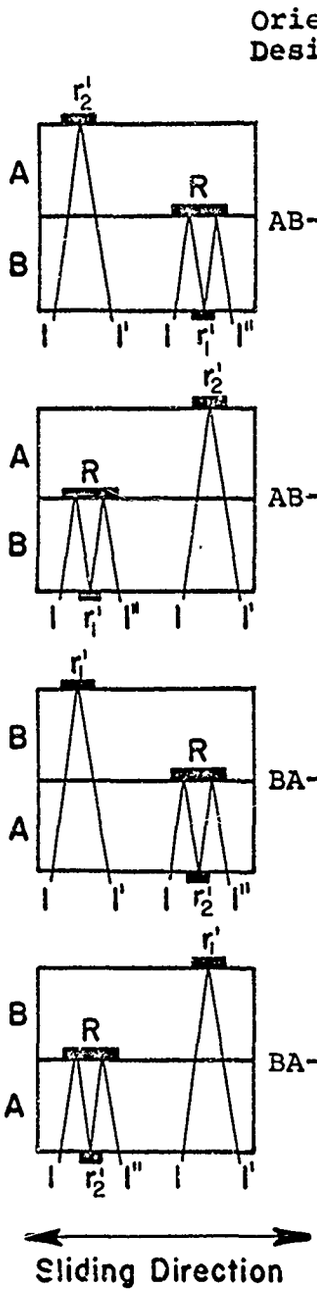

$$a = \left(\frac{I''/I}{I'/I}\right)^{\frac{1}{2}} = \left(\frac{R^2 r_1'}{r_2'}\right)^{\frac{1}{2}} = R\left(\frac{r_1'}{r_2'}\right)^{\frac{1}{2}}$$

$$b = \left(\frac{I''/I}{I'/I}\right)^{\frac{1}{2}} = \left(\frac{R^2 r_1'}{r_2'}\right)^{\frac{1}{2}} = R\left(\frac{r_1'}{r_2'}\right)^{\frac{1}{2}}$$

$$c = \left(\frac{I''/I}{I'/I}\right)^{\frac{1}{2}} = \left(\frac{R^2 r_2}{r_1'}\right)^{\frac{1}{2}} = R\left(\frac{r_2'}{r_1'}\right)^{\frac{1}{2}}$$

$$d = \left(\frac{I''/I}{I'/I}\right)^{\frac{1}{2}} = \left(\frac{R^2 r_2'}{r_1'}\right)^{\frac{1}{2}} = R\left(\frac{r_2'}{r_1'}\right)^{\frac{1}{2}}$$

Reflectivity of specimen

$R = (abcd)^{\frac{1}{4}}$

$r' =$ and $r_2' =$ Reflectivity of standard mirrors

Light path plane was rotated 90 degrees relative to the blocks in order to show the relations.

Figure 5. Four Orientations of Specimen.

mirrors and to compensate for the geometrical effects of the block surfaces. By taking the products of the ratios measured in four orientations, the absolute reflectivity of the specimen can be obtained even if the reflectivities of the standard mirrors mounted on the two blocks are not exactly equal.

For 1% noise level of the output signal, the uncertainty of the final results of the reflectivity measurements based on the radiant flux ratio can be estimated as follows:
For each of the orientations of the blocks, reflectivity is given by

$$R_i = (I''/I')^{\frac{1}{2}}$$

Following Kline and McClintock (35), for uncertainties in single-sample experiments, the uncertainty of R_i, ΔR_i, is

$$\Delta R_i = \left[\left(\frac{\partial R_i}{\partial I''} \Delta I''\right)^2 + \left(\frac{\partial R_i}{\partial I'} \Delta I'\right)^2\right]^{\frac{1}{2}}$$

$$\Delta R_i = \left\{\left[\tfrac{1}{2} \left(\frac{I'}{I''}\right)^{\frac{1}{2}} \frac{1}{I'} \Delta I''\right]^2 + \left[\tfrac{1}{2} \left(\frac{I'}{I''}\right)^{\frac{1}{2}} \frac{I''}{(I')^2} \Delta I'\right]^2\right\}^{\frac{1}{2}}$$

For $R_i \approx 1$ $\quad I'' \approx I'$

$$\frac{\Delta R_i}{R_i} = \left\{\left[\frac{1}{2} \frac{\Delta I''}{I''}\right]^2 + \left[\frac{1}{2} \frac{\Delta I'}{I'}\right]^2\right\}^{\frac{1}{2}}$$

and for $R_i \approx 1$, $\frac{\Delta I''}{I''} = \frac{\Delta I'}{I'} = \frac{\Delta I}{I}$

therefore

$$\frac{\Delta R_i}{R_i} = 2^{-\frac{1}{2}} \left(\frac{\Delta I}{I}\right) = 0.007$$

since 1% noise level has been assumed $\left(\text{i.e. } \frac{\Delta I}{I} = 0.01\right)$.

The final results of reflectivity is calculated from observations on four different orientations. It is expressed as

$$R = (R_1 R_2 R_3 R_4)^{\frac{1}{4}}$$

Following Kline and McClintock (35), the uncertainty of R, ΔR, is

$$\Delta R = \left[\left(\frac{\partial R}{\partial R_1} \Delta R_1\right)^2 + \left(\frac{\partial R}{\partial R_2} \Delta R_2\right)^2 + \left(\frac{\partial R}{\partial R_3} \Delta R_3\right)^2 + \left(\frac{\partial R}{\partial R_4} \Delta R_4\right)^2\right]^{\frac{1}{2}}$$

$$\Delta R = 2 \frac{\partial R}{\partial R_1} \Delta R_1$$

since it is quite safe to assume that each term in parenthesis gives the same value.

Thus

$$\Delta R = 2 \cdot \frac{1}{4} \left(R_1 R_2 R_3 R_4\right)^{\frac{3}{4}} R_2 R_3 R_4 \Delta R_1$$

$$\frac{\Delta R}{R} = \frac{1}{2} \frac{\Delta R_1}{R_1}$$

$$\frac{\Delta R}{R} = 0.0035 \left(\text{since } \frac{\Delta R_1}{R_1} = 0.007\right)$$

$\Delta R = 0.0035$ when $R \approx 1$

Thus, the uncertainty of each data point is expected to be about 0.0035 reflectivity unit assuming an estimated uncertainty in the output signal measurement of 1%. In reality this is larger than the observed uncertainty which falls within ± 0.002.

V. DESCRIPTION OF THE APPARATUS

A. General Features

An apparatus was designed and constructed to measure the normal spectral reflectivity by using the multiple reflection technique in the infrared region, 2 to 13 microns, in air and at room temperature. The angles of incidence and reflection are fixed at seven degrees from the normal to the specimen surface. The apparatus consists of the conventional Perkin-Elmer 12-C single beam single pass infrared spectrometer, transfer optics, specimen holder, and recorder. The block diagram and general arrangement of the system are shown in Figures 6 and 7, respectively.

B. Specimen Holder

The specimen holder is composed of two identical blocks, A and B, made of stainless steel 304. The overall dimensions for each block is 3.75 X 3.75 X 2.0625 inches. Two cut-outs are made for the light path. The upper and lower surfaces of each block are machined parallel to each other within 0.0005 inch. Both the inside and the outside walls of the blocks are sprayed with 3M velvet black coating to minimize reflected stray energy. The blocks are connected to each other with two positioning pins, and either of which may be

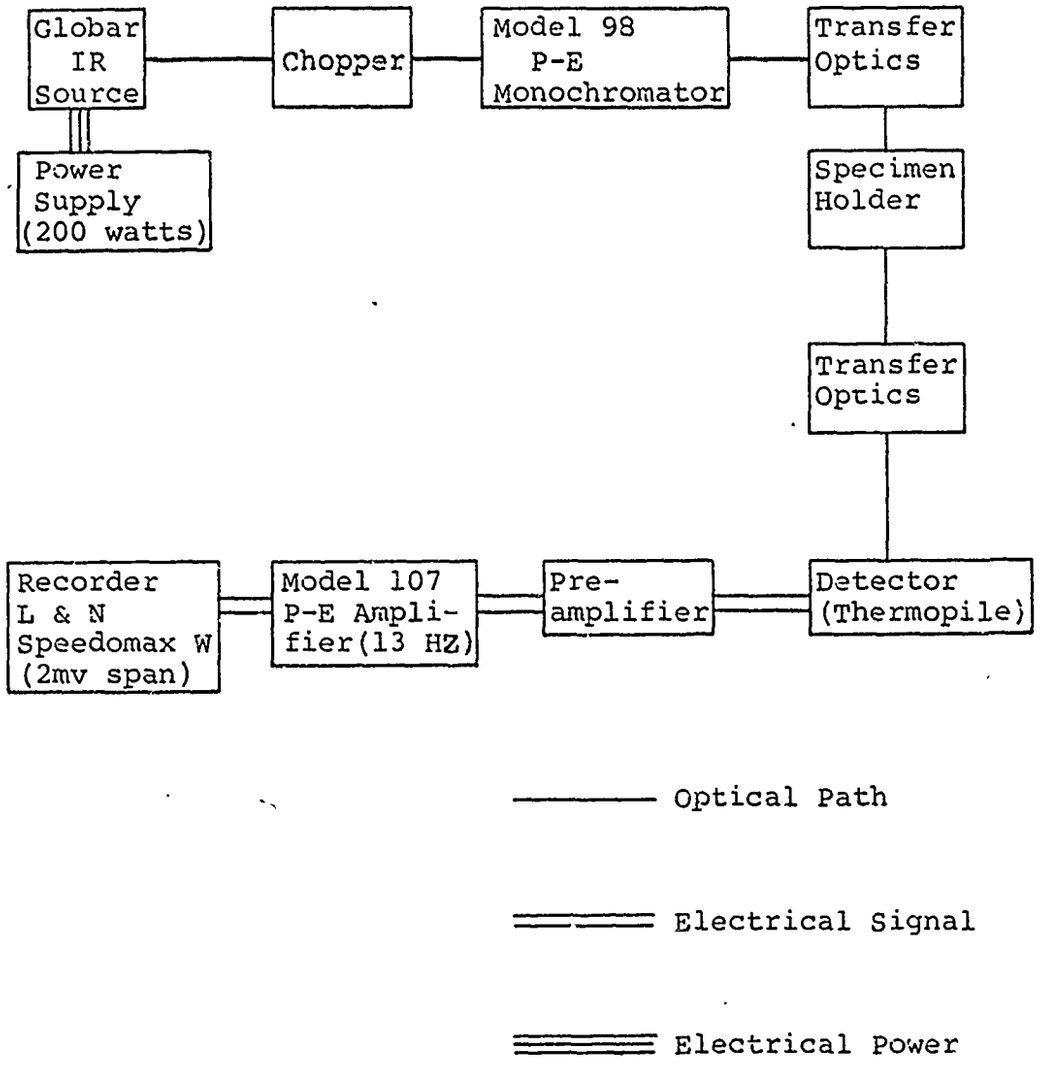

Figure 6. Block Diagram of the System Used in the Present Study.

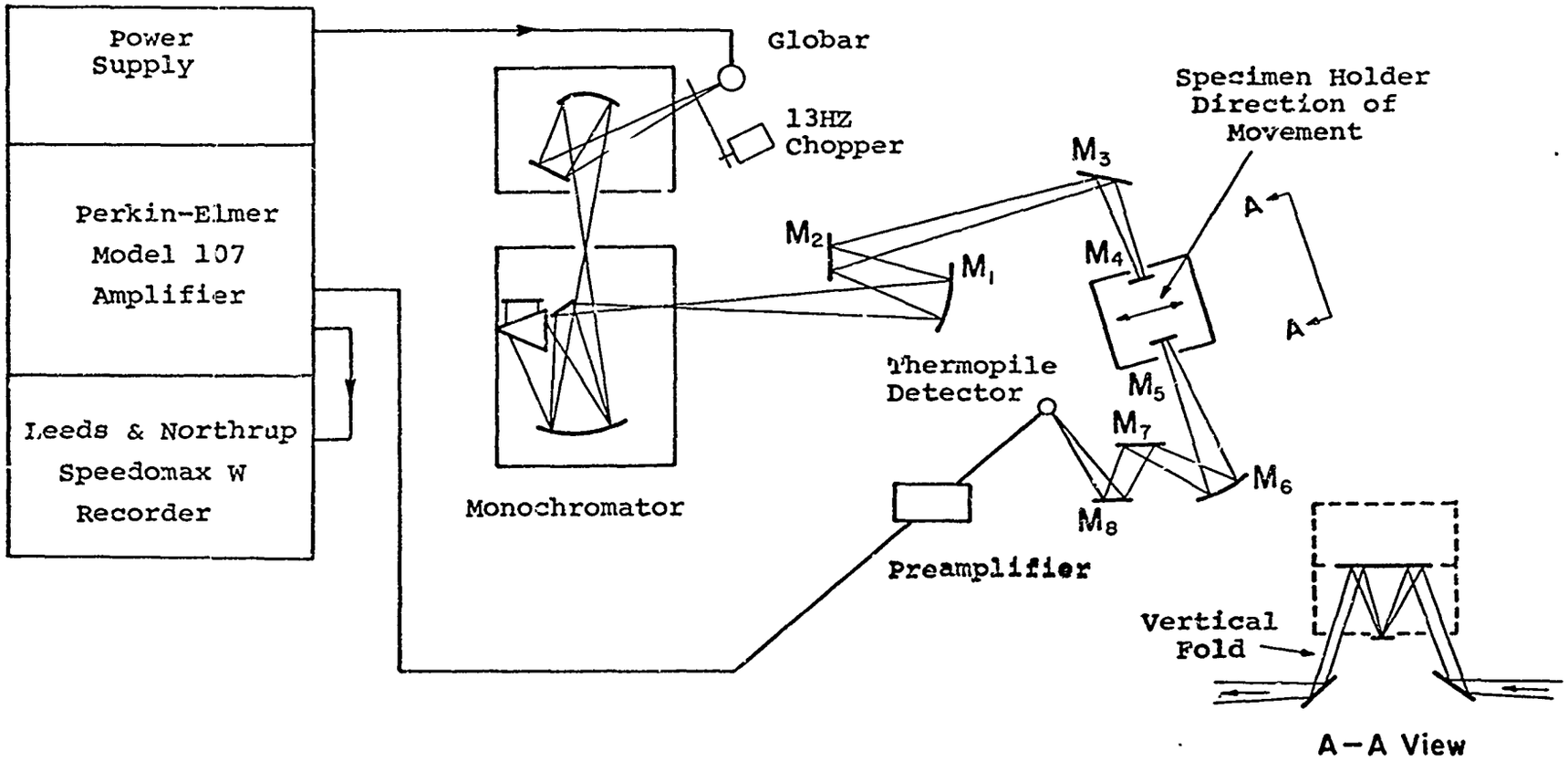

Figure 7. Schematic of Apparatus For Measurement of Absolute Normal Spectral Reflectivity.

placed on top of the other. The two standard mirrors (Electroplated, first surface rhodium plane mirrors, size 1/2 x 1 3/8 inches, Evaporated Metal Films Corporation, Ithaca, New York) and the specimen under study are mounted by clip springs on the surfaces of the blocks. The rhodium mirrors are chosen because their reflectance values in air are quite stable (29,43). The specimen holder and the locations of specimen and standard mirrors are shown in Figures 8 and 9.

The specimen holder can be manually slid on a supporting base to positions of SPECIMEN IN and SPECIMEN OUT. The positions are located by stops at the two ends of the supporting base with adjustable screws for alignment. The supporting base is in turn supported by three brass columns which are fastened on a leveling base which can be adjusted by three pairs of screws for optical alignment.

C. The Transfer Optics

Figure 7 and Table 1 indicate the transfer optics, their dimensions, and relative distances. All transfer optics are first surface aluminum mirrors. The exit slit is imaged on the standard mirror on the specimen holder by 1:2 ratio and re-imaged by 1:1 ratio on the detector. The average angle of incidence on the surface is about 7°. The horizontal folding of the infrared beam is necessary because of the limited space of the base plate of the optical bench on which all the mirrors, monochromator, and the specimen

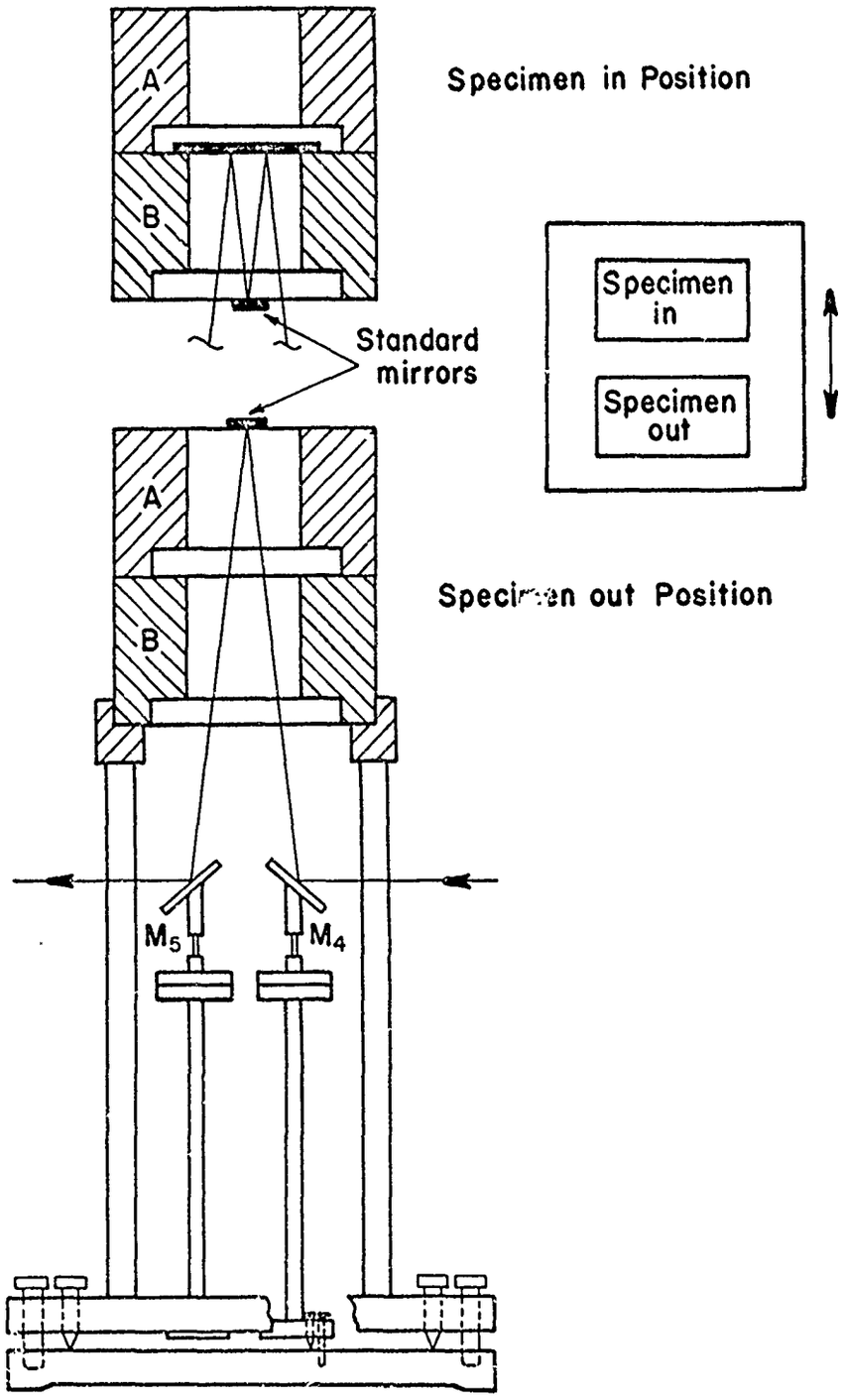

Figure 8. Sketch of Specimen Holder.

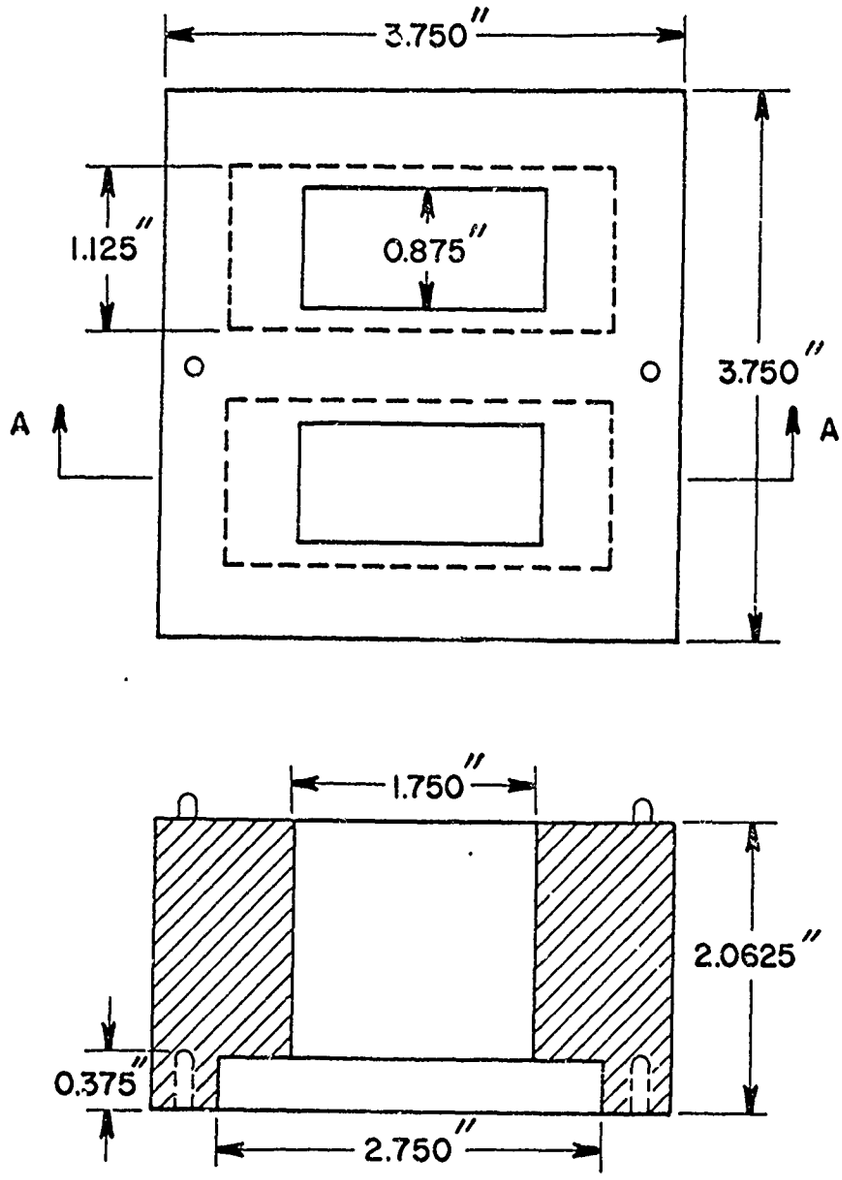

Figure 9. Dimensions of Specimen Holder Blocks A and B.

Table 1. Transfer Optics

Mirror*	Kind	Size (in.)	Focal Length (in.)	Distance[c] (in.)
M_1	S[a]	6 (dia.)	16	10[d]
M_2	D[b]	4x4		21
M_3	D	3x3		10
M_4	D	1¼x1½		14[e]
M_5	D	1¼x1½		15
M_6	S	4¼ (dia.)	11	6
M_7	D	2½x2½		6
M_8	D	2½x2½		10[f]

* All mirrors are first surface aluminized mirrors.

(a) Spherical mirror.

(b) Diagonal mirror (plane).

(c) Distance to the next mirror.

(d) The distance from the exit slit to M_1 is 24 inches.

(e) The distances from M_4 to standard mirror and from standard mirror to M_5 are both seven inches

(f) This is the distance from M_8 to the detector.

holder are mounted.

All mirror mounts are capable of being adjusted as to the height, the tilt, and the rotation of the mirror so the optics can be aligned. All mirrors are cleaned when necessary with 95% ethanol, distilled water, and absorbent cotton.

D. P-E 12-C System

The conventional Perkin-Elmer 12-C single beam, single pass, infrared spectrometer with a chopper in front of the globar source, is used. The globar, operated at about 1100^{o}C, and the NaCl prism give the desired radiation with wavelengths ranging from two to 13 microns.

The two bilateral slits (entrance and exit slits) in the P-E Model 98 monochromator are each 12 millimeters high which is reduced to two millimeters by baffles installed near the slits. The slits are operated simultaneously by the slit micrometer which reads directly in microns from zero to two millimeters.

E. The Detection System

The detector used in this experiment is a Charles M. Reeder & Company, Inc., No. RP3-W thermopile with KBr window and 18 ohms resistance. The receiver area is 6.0 x 0.4 millimeters. The output is amplified and rectified by a Perkin-Elmer amplifier (Model 107) and monitored on a Leeds & Northrup Recorder (Model Speedomax W, single point, multiple range, multiple speed, strip chart).

The entire optical system is within a black cloth

enclosure which prevents dust deposits and prevents the detector from receiving stray light which tends to increase the noise of the detector output.

Flux averaging spheres, with two and three inches diameter and coated inside with crystex sulfur (18), are fabricated and can be mounted over the detector (see Appendix C).

VI. CALIBRATION OF THE APPARATUS

A. General Features

After the system was fabricated, the optics were properly aligned. The apparatus was calibrated on its slit width, wavelength, and linearity. The standard comparison is then made and performance checked.

The optical alignment of mirrors and specimen holder was accomplished by setting the monochromator so that the visible part of the spectrum was focused on the exit slit. In place of the standard mirror a greased piece of paper was installed. The image of the exit slit was visually focused at the center of the paper by adjustments of the mirrors, adjustable screws on the supporting base of the specimen holder and the leveling screws of the specimen holder. Subsequently, the greased piece of paper was installed right in front of the detector. The image of the exit slit was again caused to fall on the same location for SPECIMEN IN and SPECIMEN OUT conditions. Since the spherical mirrors were used off-axis, the image of the exit slit was slightly astigmatic. Optical alignment was made such that the desired location was the circle of least confusion. The tangential and sagittal images were located very close to

the specimen surface.

B. Slit Width Linearity

Although no occasion was anticipated to compare energies with different slit widths, it was still necessary to check the slit width linearity to verify proper operation of the monochromator including resolved slit width.

For optimum alignment the square root of the radiative energy emerging from the exit slit should be proportional to the slit width setting (see Appendix A). The performance was checked at a wavelength of about 2.25μ. At this wavelength the globar source gives the highest energy and hence, small slit widths could be used. For each amplifier gain (gains of 4-0, 6-0, 9-0, 12-3), the slit width was varied and the pen deflections were recorded. A plot of the square root of the pen deflection against the slit width is shown in Figure 10. The fairly good linear relation indicates the good alignment of the monochromator slits and optics.

C. Wavelength Calibration

The drum on the monochromator has 100 divisions for each turn with total of 24 turns. The correspondence between the drum number and wavelength is unique for every instrument since it varies for each individual prism. Therefore, it is necessary to obtain a wavelength calibration curve for the experimenter's particular instrument.

The calibration is in principle a function of

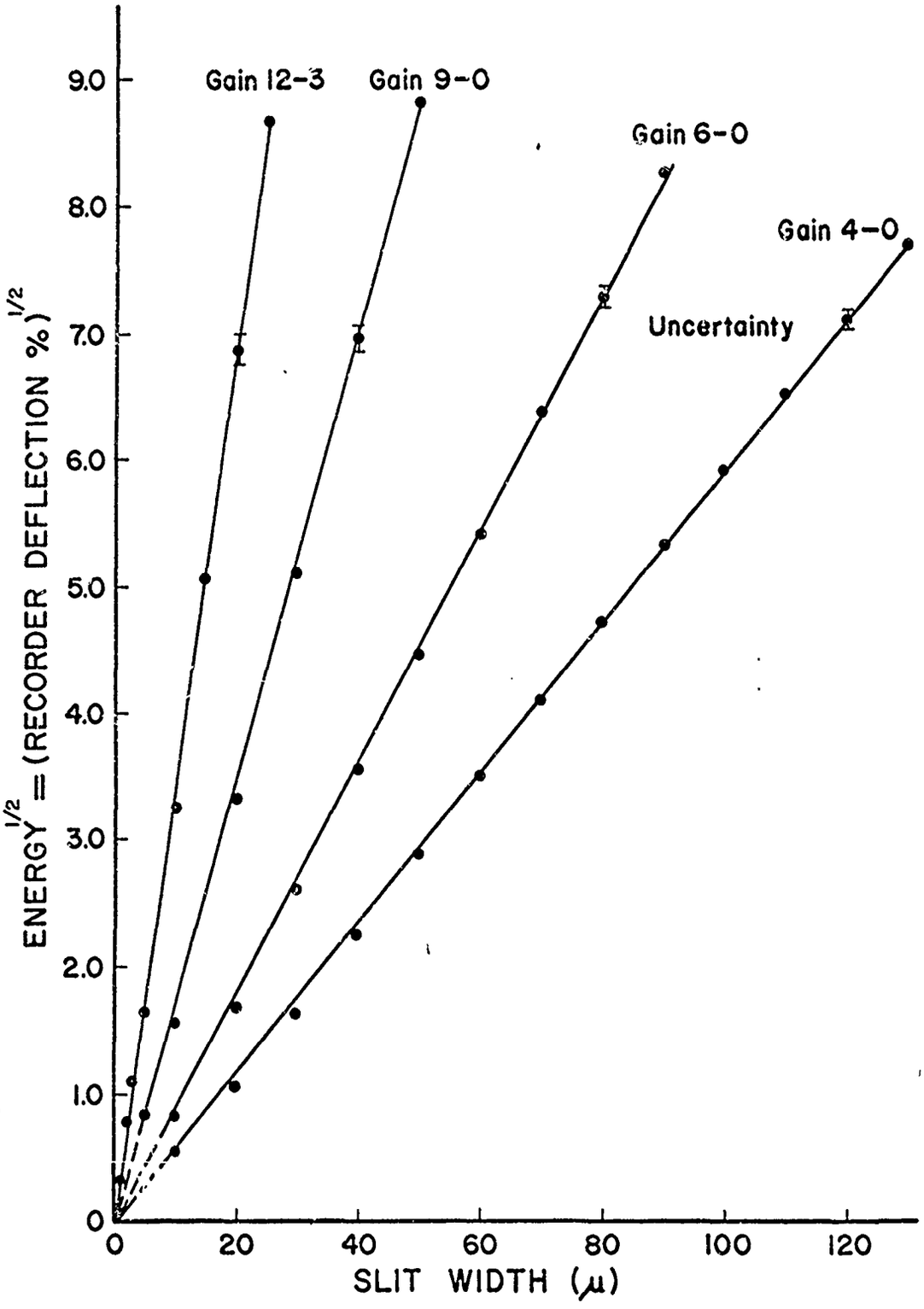

Figure 10. Monochromator Slit Width Linearity Performance Curve

temperature of the prism. The magnitude of the temperature effect for any prism may readily be estimated by comparison of the variations of the refractive index with wavelength and with temperature. The temperature immediately adjacent to the NaCl prism inside the monochromator has been checked and the temperature was found to be controlled at $99^{o}F \pm 1^{o}F$ during the three days' checking. Because the temperature of the prism is well controlled within $\pm 1^{o}F$ and the temperature compensating device is included in the monochromator, it is expected that once the wavelength calibration is established, there will be no change of this calibration due to temperature effect.

Absorption bands with known wavelength of polystyrene (41), H_2O and CO_2 in atmosphere (39) are used for the calibration. The drum is driven automatically with specified scanning speed to scan over the entire spectrum. Drum numbers for minimum pen deflection are read precisely by using the wavelength marker which gives a short line on the recorder for each drum division. The corresponding wavelengths, drum numbers, together with the operation conditions are given in Table 2 and plotted in Figure 11. The corresponding drum numbers for wavelengths from two microns to 13 microns obtained from the smoothed calibration curve in Figure 11 is given in Table 3.

Table 2. Wavelengths and Corresponding Drum Numbers Determined From Absorption Bands

(I) Polystyrene[a]

λ(μ)	Drum Number
2.170	1869.6
2.577	1848.6*
2.674	1845.2
2.763	1841.2*
3.269	1817.6
3.303	1816.2*
3.511	1806.6*
4.225	1767.8
4.281	1764.8*

(II) Polystyrene[b]

λ(μ)	Drum Number
5.138	1712.5
5.343	1699.5
5.549	1685.0
6.238	1632.5
6.692	1596.5
8.662	1405.0*
9.742	1281.0*
11.035	1107.0*

(III) H_2O in Atmosphere[c]

λ(μ)	Drum Number
5.204	1708.8*
5.356	1699.0
5.466	1690.8
5.639	1678.4*
5.762	1669.4
5.822	1665.2
5.936	1675.0
5.986	1652.8*
6.112	1643.2
6.182	1637.6
6.339	1625.2
6.427	1619.8
6.487	1613.2
6.563	1606.8*
6.633	1601.6
6.709	1595.4
6.786	1588.4
6.856	1582.2
6.961	1573.4
7.044	1565.4*
7.165	1554.8*

(IV) CO_2 in Atmosphere[d]

λ(μ)	Drum Number
13.879	641.0*

(a) Slit width 0.016 mm., amplifier response 2, drum speed rev./4 min.

(b) Slit width 0.300 mm., amplifier response 1, drum speed rev./2 min.

(c) Slit width 0.036 mm., amplifier response 2, drum speed rev./4 min.

(d) Slit width 0.300 mm., amplifier response 2, drum speed rev./2 min.

* Data used to plot the calibration curve in Figure 11.

Note (1): Settings of wave drum were always made toward increasing drum number.

Note (2): Polystyrene sheet was made by Beckman, Inc.

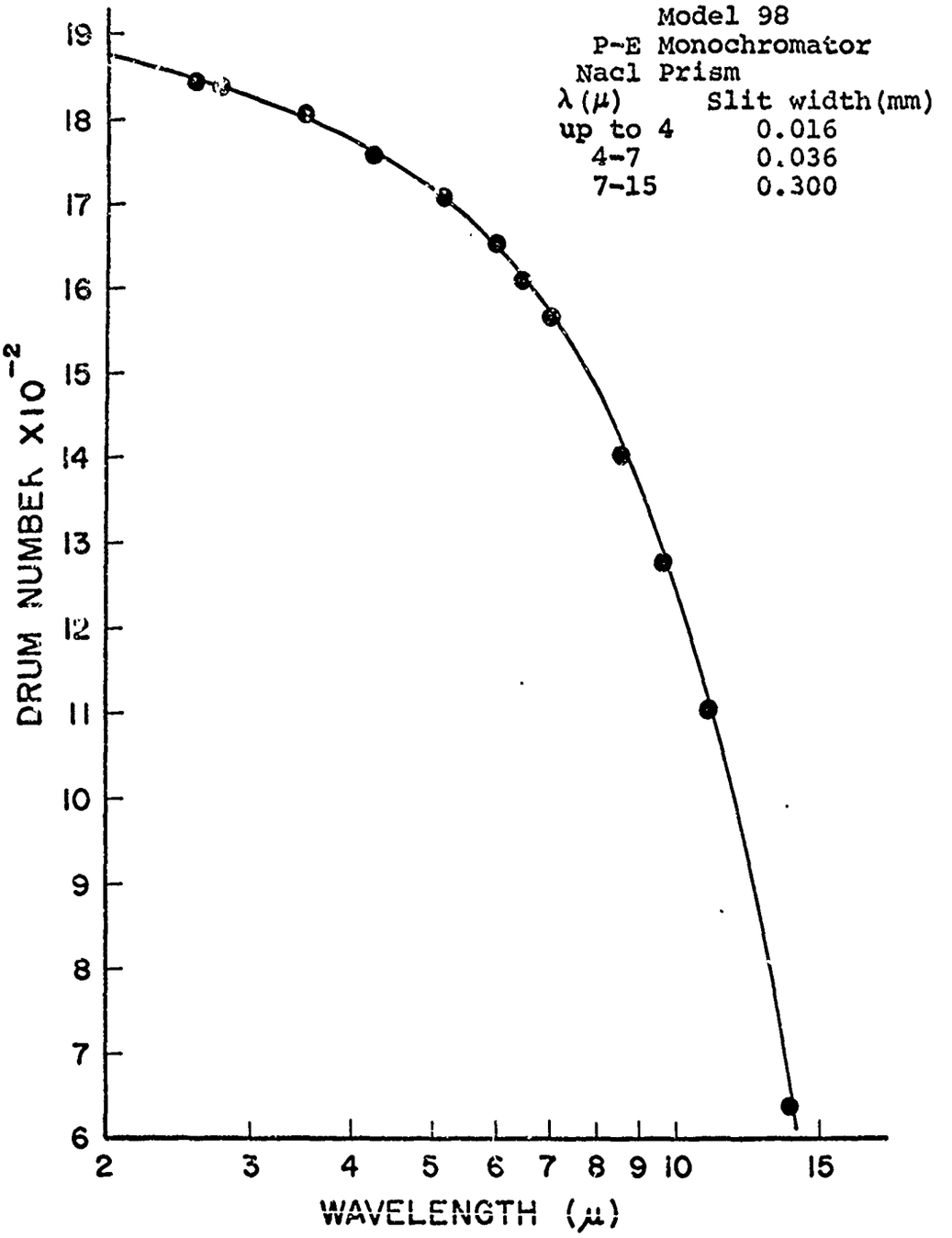

Figure 11. Wavelength Calibration of the Monochromator with NaCl Prism.

Table 3. Monochromator Wavelength Calibration.

$\lambda(\mu)$	Drum Number
2	1875
3	1830
4	1781
5	1722
6	1652
7	1565
8	1475
9	1368
10	1250
11	1120
12	970
13	800

D. Linearity

Reflectivity determination requires radiant flux measurements. If really accurate measurements are to be made, it is necessary that either the output signal from the instrument be strictly proportional to the incident radiant flux, or that the departure from linearity be known and corrections be made. The linearity of different stages of electronics may be checked by introducing calibration signals into the recorder and the preamplifier inputs and measuring the output signal. The linearity of the complete system (detector and electronics) may be checked by introducing into the light path some device which gives known transmittance.

1. Recorder Linearity Calibration

The linearity calibration was performed by using a dc source (with 10 ohm output impedance) to get the recorder indicator on 100%, 90%, ---, and 0% on the L&N Speedomax W recorder with two millivolt full scale. The true voltage value was read from the potentiometer and the procedure was repeated with increasing dc source output.

The calibration curves for both settings are shown in Figure 12. The differences between the readings of Recorder (%) and True (%) are well within the $\pm$0.3% specified in the instrument manual.

Other possible instruments for readout of the output are digital voltmeter (DVM) and voltage-frequency converter with counter (6). In the case of the counting technique the setting precision can be as good as 0.025%.

Due to the noise of the output signal it was difficult to observe the output signal on the displacing screen of the above-mentioned two instruments and obtain an average value. On the recorder, however, an average value was rather easy to obtain from the output curves on the chart paper. Thus, in this experiment the recorder was employed.

2. Amplifier-Recorder Linearity Calibration

The test microvolts supplied by the setting of the P-E 107 amplifier dials are not accurate because of the uncertainty ($\sim \pm$10%) of the resistors used in the test microvolt circuit and the voltage variation of the battery. A

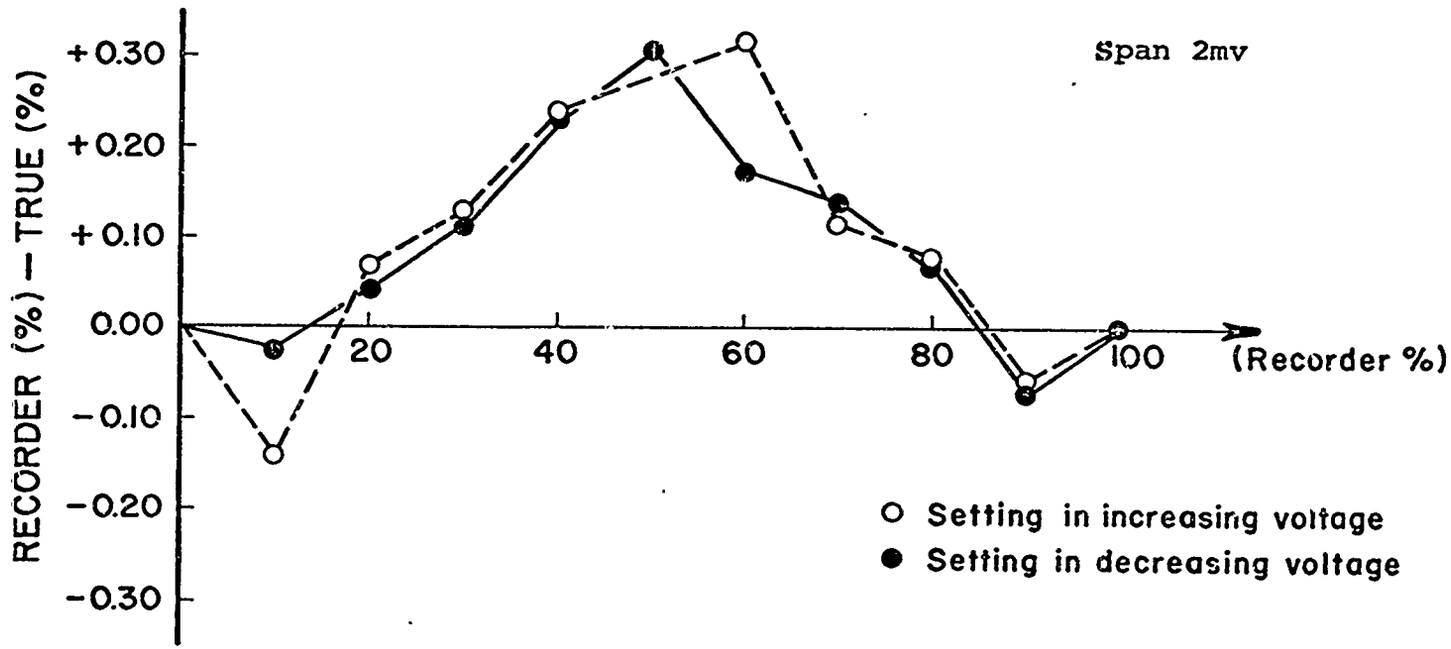

Figure 12. Linearity Characteristic of the Recorder.

precision resistor box* and a 2.1 volts low self-discharge rate storage battery were used to replace the dry battery and test resistors in the P-E 107 amplifier. Accurately known small signal increments can then be introduced at the input to the preamplifier.

The Dekabox setting and corresponding True % are shown in Table 4. The calibration results are shown in Figure 13

Table 4. Amplifier-Recorder Linearity Dekabox Setting

R(KΩ)	True %
10	100
12.5	80
16	62.5
20	50
25	40
40	25
50	20
100	10
open	0

for both increasing and decreasing voltage settings. The apparent (%)-True (%) are within ±0.2%.

3. Detector-Amplifier-Recorder Linearity Calibration

The final calibration required is that of the linearity of the complete system (detector and electronics). This calibration can be made for the thermopile detector by using

*Model DB 655 Dekabox decade resistors are double coaxial-dial precision resistance elements manufactured by Electro Scientific Industries, Inc., Portland, Oregon. The accuracy for 10^3 ohms to 10^6 ohms is 0.01%.

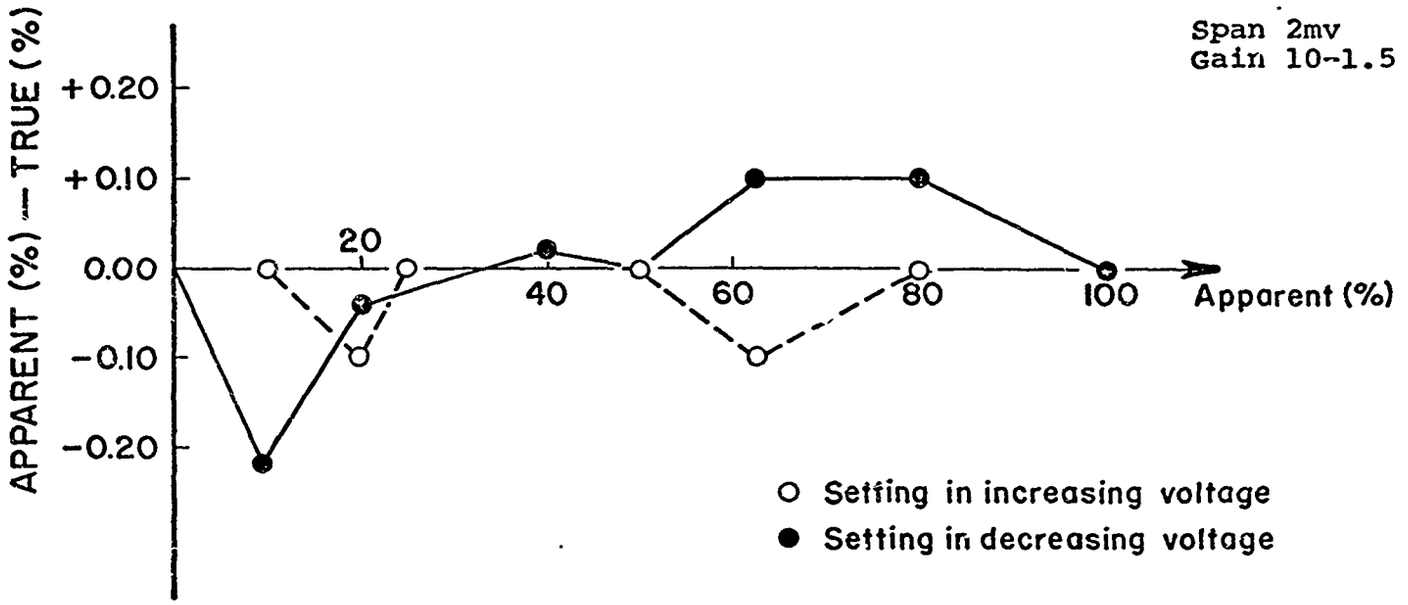

Figure 13. Linearity Characteristic of the Amplifier-Recorder Combination.

a set of sector-disc attenuators similar to the set described by Harrison, et al., (28). The discs are the same as used by Zipin (5) with the detailed dimensions and true transmissions given in Table 5.

Table 5. True Transmission of the Sector-Disc Attenuators

Nominal Transmission of Disc (%)	Diameter (in.)	Sum of Notches Angle $\Sigma\theta$	True Transmission T(%)	No. of Notches	Uncertainty Δ[T(%)]
5	10	$22^{\circ}27'$	6.24	4	$\pm$0.0185
12.5	9	$43^{\circ}46'$	12.16	8	$\pm$0.0370
25	9	$90^{\circ}9'$	25.58	8	$\pm$0.0370
50	9	$185^{\circ}42'$	51.58	8	$\pm$0.0370
75	9	$271^{\circ}10'$	75.32	8	$\pm$0.0370

To perform the calibration, the specimen holder is set in the SPECIMEN OUT position and the amplifier gain is adjusted to bring the recorder deflection to near full scale. The discs are put in the optical path, between M_3 and M_4, in turn and driven with a motor* at a high enough speed (~1400 rpm) so that no coupling is observed between the sectored disc and the chopper. The discs are not put right in front of detector so there will be no thermal radiation falling on the detector directly due to the presence of the motor and disc blades to increase the noise. The recorder deflection due to each of the discs rotating in the optical

*Manufactured by Precision Scientific Co., Chicago, Illinois. The motor is turning counterclockwise and the chopper blade is turning clockwise when observed along the optical path.

path is compared with the 100% reading to calculate the apparent transmission. They are plotted as [T apparent (%) - T true (%)] vs (T apparent) in Figure 14. The non-linearity is about ±0.6%.

The operation principle of the attenuator is that the radiation energy arriving at the thermopile detector is blocked by the rotating blades of the attenuator part of the time. The portion of the unblocking time determines the transmission. There is an inherent uncertainty involved in using the attenuator as a device to check the linearity because of the slower response time (comparative to electronics) of the thermopile. That is, the real transmission caused by the attenuator may never be the same as the true transmission value given in Table 5, no matter how small the uncertainty of the angles of the blades can be determined. It may seem possible at the first thought to make these two transmissions identical by using a slower speed of the attentuator motor. But in this way, the coupling effect with the chopping blades in front of the source increases the noise of the output signal and thus increases the uncertainty of the linearity determination.

The other devices not involving rotating discs, such as standard filters, although not handicapped by the uncertainty mentioned above, still yield systematic errors (3). Still another device, the line screen (or mesh screen) does not give rise to most of the systematic errors, but it is

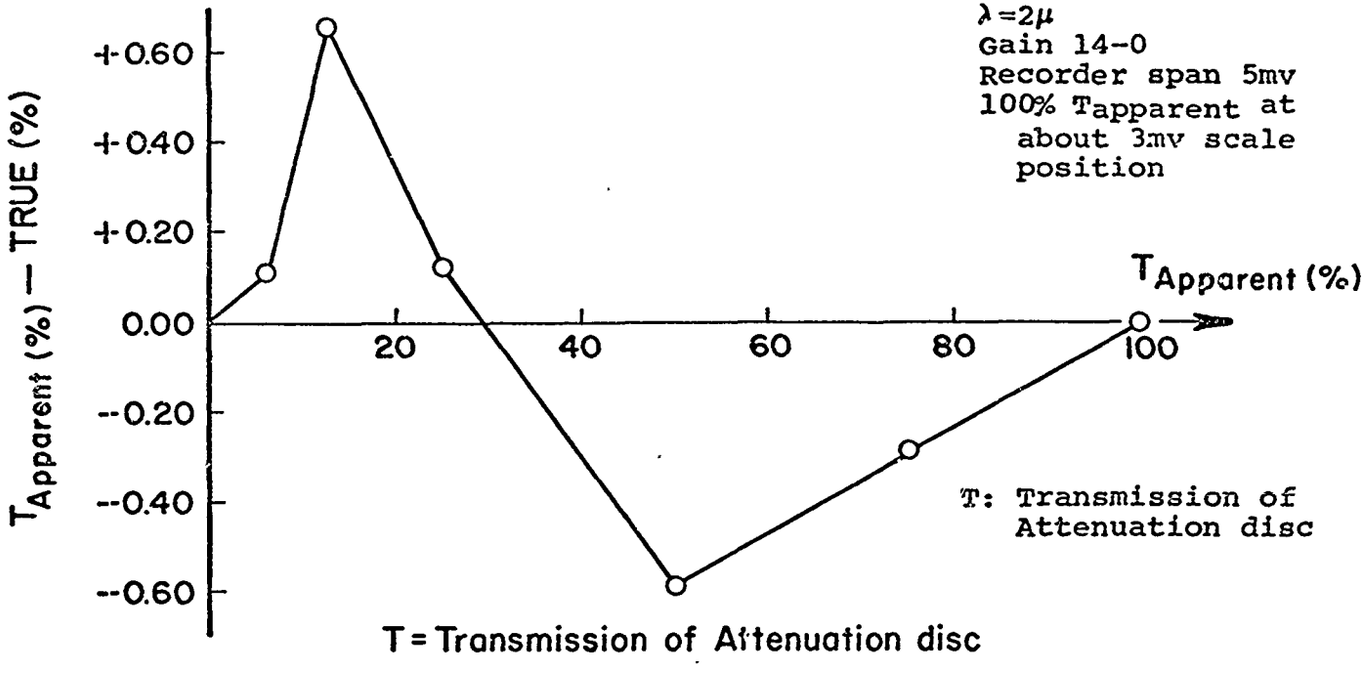

Figure 14. Linearity Characteristic of the Detector System.

very sensitive to the convergence angle of the optical beam. Thus, by these three above-mentioned devices, it is difficult to determine linearity to better than 1% or 2%. The most promising device is a system employing three optically excellent, high-extinction polarizers*(3). The common sources of the systematic error are eliminated and the linearity can be determined to better than 0.1%.

E. Stray Energy (23)

Stray energy may often cause important errors in spectrometry. The stray energy emerging from the exit slit along with the desired spectral energy may be a general admixture of energy of all wavelengths emitted by the source and transmitted by the spectrometer.

Stray energy was checked by using numbers 210 and 240 infrared filters purchased from Eastman Kodak Company. Both were two inches in diameter x 0.04 inches thick. No. 210 and No. 240 infrared filters are filters without polystyrene protective coating with 1μ and 4μ cut-on wavelength**, respectively. The infrared filter was placed in front of the entrance slit of the monochromator during the measurements. The No. 210 filter was used for the wavelength range two to five microns; while the No. 240 filter was used in the seven to 13 micron range.

---

* An instrument employing such optical elements is called the Linearity/Transmittance Standards (L/TS) now in production by Technometrics, Inc., West Lafayette, Indiana.

**The cut-on wavelength is defined as the wavelength at which the transmission reaches 3%.

Reflectivity of aluminum specimen No. Al-B1 was measured with and without filter from two to 13 microns. No trend of difference can be detected from the results (see Figure 15) measured with these two conditions. Since rhodium has lower reflectivity value, the reflectivity of rhodium specimen No. 1 was thus measured with and without filter in the wavelength range seven to 13 microns (see Figure 16) in order to check whether there exists any difference

The results of the reflectivity measurements with and without the filter all fall within the experimental uncertainty, indicating that the stray energy emerging from the exit slit is negligible. Similar experience is reported by Edwards and deVolo (19) with this type of apparatus.

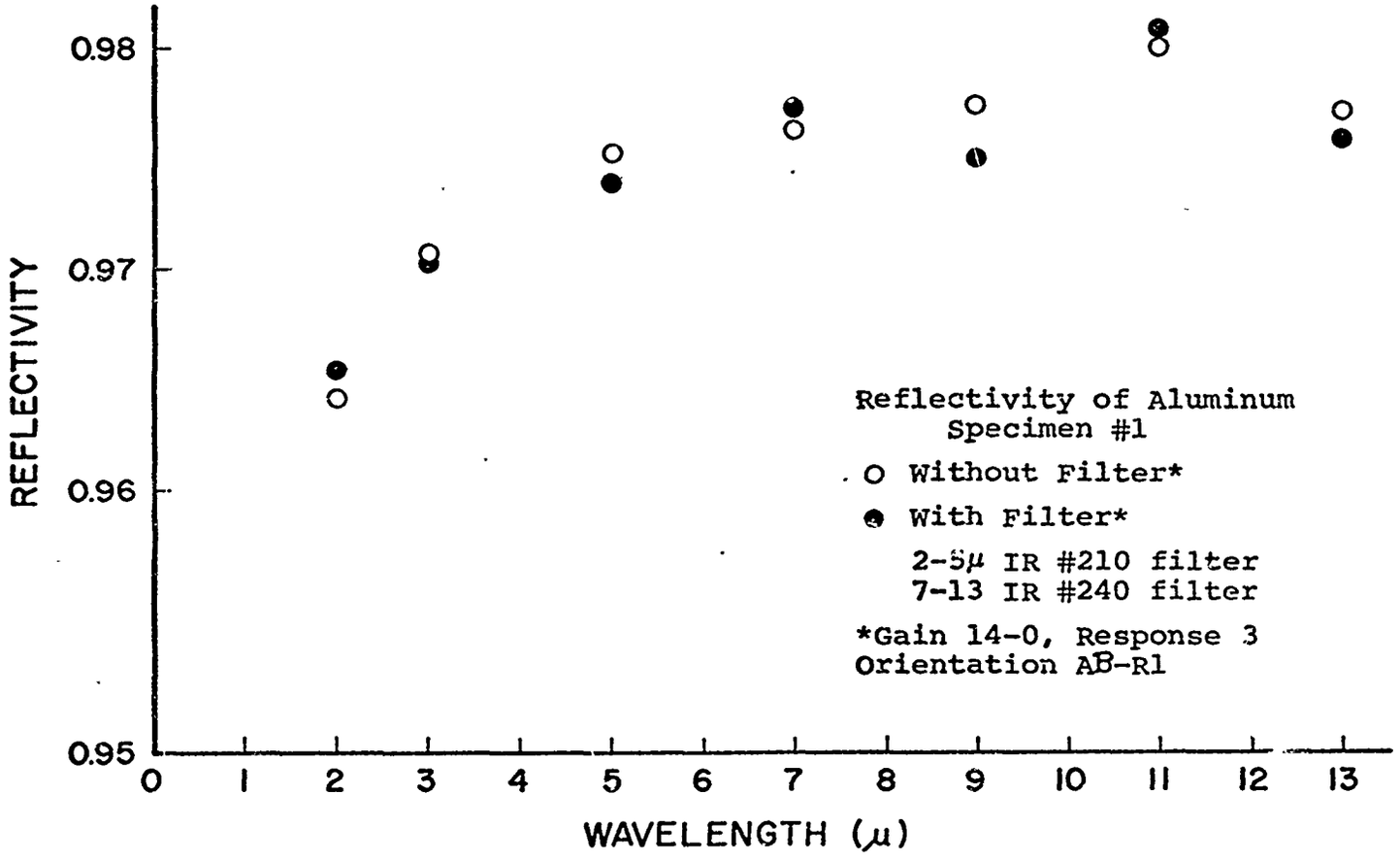

Figure 15. Stray Energy Determination
(Al Reflectivity)

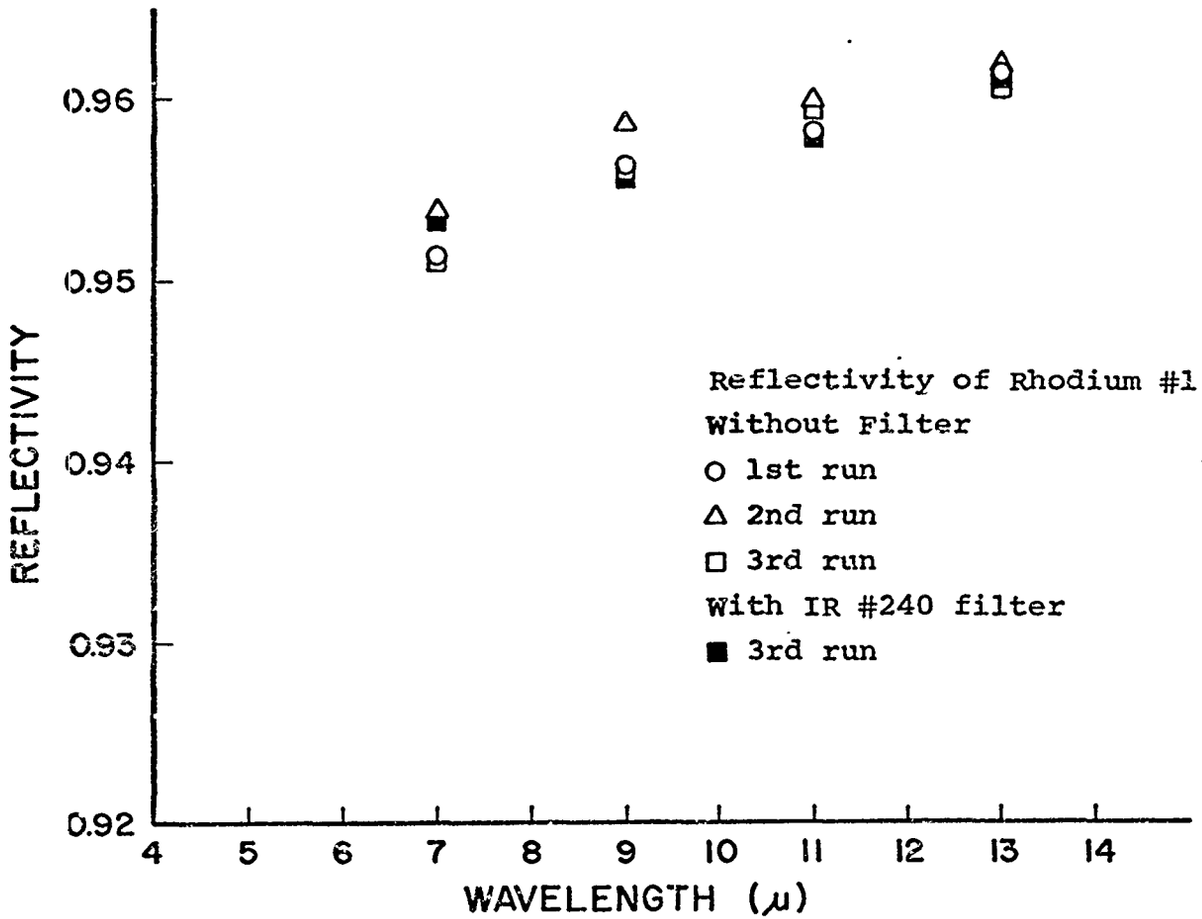

Figure 16. Stray Energy Determination
(Rh Reflectivity)

VII. EXPERIMENTAL PROCEDURE

Upon completion of the alignment and calibration of the apparatus, the standards comparison and performance check were then made. After the surface preparation of the specimens, the measurements on the specimens were performed. The standards comparison and surface preparation will be discussed in Chapters VIII and IX.

The whole electronic instrumentation system (except the globar source) was kept on during the entire measuring period to avoid any possibility of transient effects. After turning on the globar source, there was usually a wait of approximately one hour before it reached steady state. The stability of the globar source was checked by observing minimum pen deflection on the recorder for a ten minute period.

First, the specimen and two small standard mirrors were mounted on the specimen holder for the orientation AB-R1. The "zero" position on the recorder, i.e. with shutter in front of the entrance slit closed and detector uncovered, was then set by adjusting the BALANCE dial on the amplifier. A two millivolt span was used on the recorder and one millivolt was suppressed.

The desired wavelength drum setting, slit width, and amplifier gain were set, and the pen deflections for SPECIMEN

IN and SPECIMEN OUT positions, as described in Chapter V, were recorded for each wavelength. Measurements were performed for wavelengths 2,3,4,5,7,9,11, and 13 microns. The slit width setting varied from 0.080 millimeters at two micron wavelength to 1.58 millimeters at 13 microns corresponding to 0.035 micron and 0.28 micron resolved bandwidth, respectively (see Appendix B). After all three specimens were measured for one block orientation, the same procedure was carried out for the other three orientations. Every specimen was measured within eight hours after surface preparation.

The flux averaging spheres, two and three inch diameters with crystex sulfur coating, were tried over the detector. The output was too small especially at the longer wavelengths (see Appendix C). Therefore, it is hard to obtain an adequate value to calculate the radiant flux ratio precisely. Thus, all the measurements were made without the flux averaging sphere. A source of error arising from spatial sensitivity of the detector cannot be avoided. Hence, the determination of measurement accuracy and precision is strongly required and will be discussed in the following section "Standards Comparison and Performance Check."

The data reduction procedure is as follows. For each specimen the reflectivity was measured as a function of wavelength. For every orientation and at each wavelength the reflected energy of SPECIMEN IN and SPECIMEN OUT were recorded to calculate the normal spectral reflectivity. Since the

same amplifier gain was used for SPECIMEN IN and SPECIMEN OUT positions, no determination of instrument response constant was needed.

In this experiment the recorder was adjusted to zero when the shutter in front of the entrance slit was closed. Thus, the dc signal due to the unwanted, scattered radiation reaching the detector and stray electrical signals were already excluded from the recorder readings. For every orientation, the normal spectral reflectivity, R_i, is calculated by

$$R_i = (D_1/D_2)^{\frac{1}{2}}$$

where D_1 and D_2 are recorder pen deflections corresponding to SPECIMEN IN and SPECIMEN OUT positions.

The final value for normal spectral reflectivity is calculated from data obtained from four different orientations

$$R = (R_1R_2R_3R_4)^{\frac{1}{4}}$$

VIII. STANDARDS COMPARISON AND PERFORMANCE CHECK

Reproducibility of the measurements was checked by comparing results of the first run and second run of the reflectivity measurements on opaque, uncharacterized rhodium specimen No. 1. Rhodium was selected because its reflectivity characteristics are very stable in air and at room temperature. The specimen was electroplated rhodium on flat glass prepared by Evaporated Metal Films Corporation, Ithaca, New York. The results of two runs are well within 0.002 reflectivity unit of each other (see Figure 17). Results are also comparable to the data reported by Hass (29).

The accuracy of the measurement technique was evaluated as follows. Three quartz flats were coated with high-vacuum evaporated aluminum* under well controlled conditions which yielded specimens of reference grade. The reflectivity of these three specimens were measured in this study two weeks and four weeks after evaporation. The average values are shown in Figure 18. A fourth specimen, prepared at the same time as the test specimens referred to above was measured immediately after evaporation at the Michelson Laboratory, and

*Prepared by Dr. H. E. Bennett, at the Michelson Laboratory, Naval Weapons Center, China Lake, California.

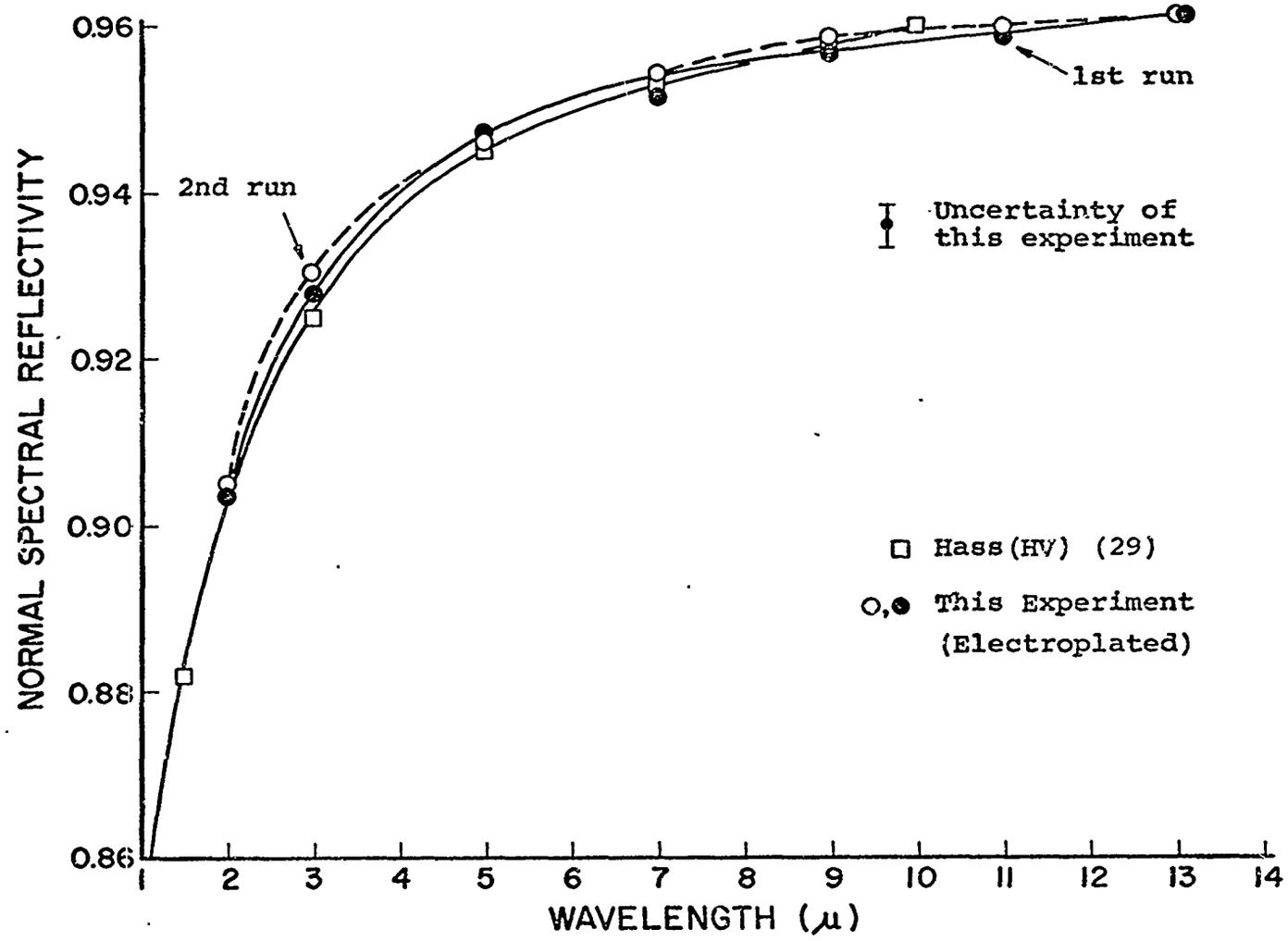

Figure 17. Reproducibility Evaluation From Measurements on The Reflectivity of Rhodium.

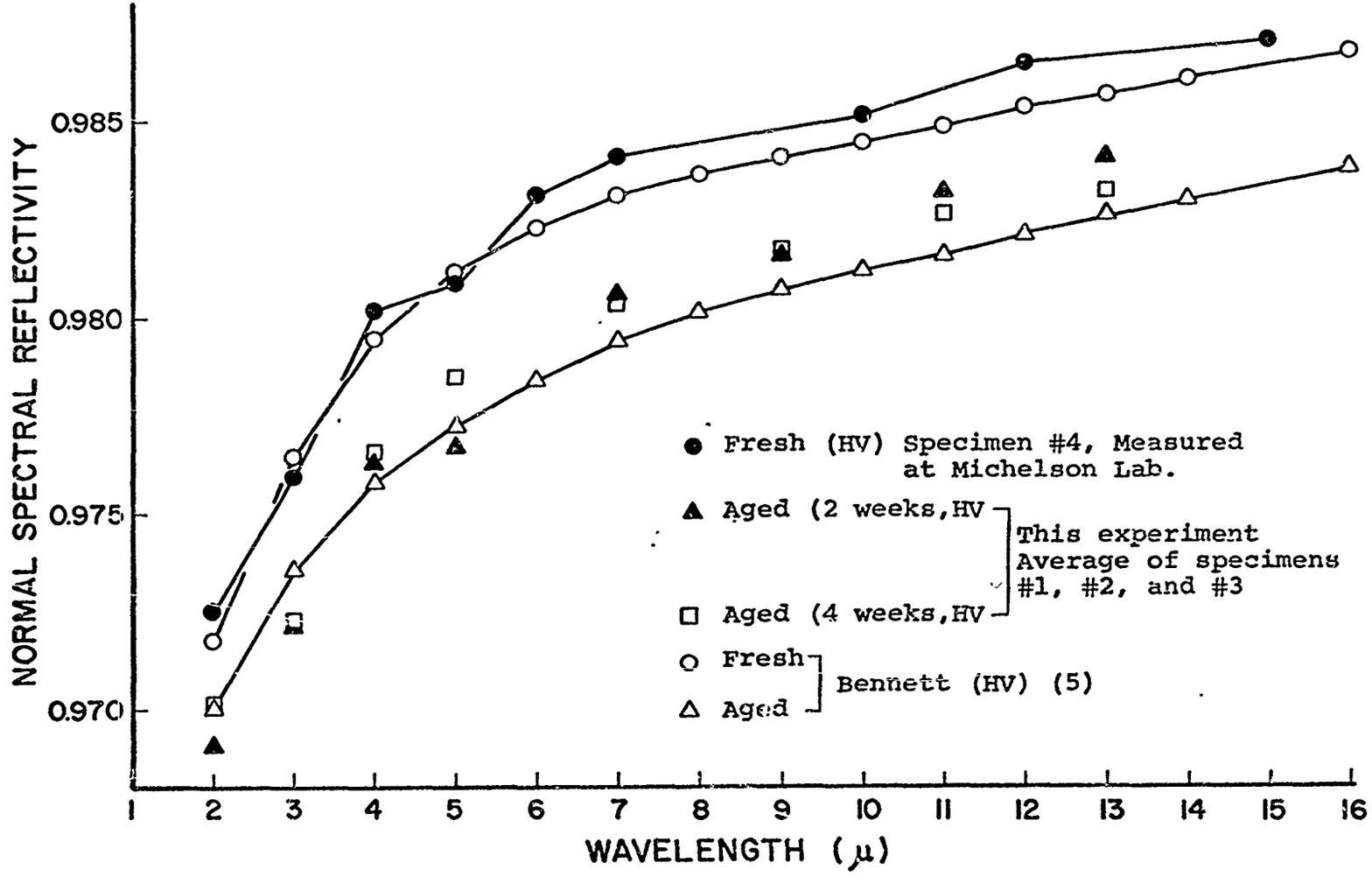

Figure 18. Accuracy Evaluation from Measurements on the Reflectivity of Aluminum.

data obtained are plotted on Figure 18, together with earlier literature values (5) on fresh and aged high vacuum evaporated, aluminized specimens. Generally, the reflectivity measurements for the condition "four weeks after evaporation" are within 0.001 reflectivity unit from those of Bennett (5) stated to have an accuracy of 0.001 unit. However, the value of reflectivity obtained in this experiment is systematically higher at the longer wavelengths. This cannot be attributed to the stray energy emerging from the exit slit since it is negligible as demonstrated in Chapter VI, "Calibration of the Apparatus."

IX. SPECIMEN PREPARATION AND SURFACE CHARACTERIZATION

A. Specimen Materials

Copper, zinc, and nickel rods 1.25 inches in diameter and two inches long were purchased from Material Research Corporation, Orangeburg, New York. The purities, as reported by the manufacturer, are given in Table 6.

Table 6. Purity of the Specimens

Material[a]	Purity(%)	Grade	Total Impurity(ppm)[c]
Copper	99.999	MARZ[b]	<33
Zinc	99.999	MARZ[b]	< 6
Nickel	99.99	VP	<123

a. Vacuum melted and cold swaged to size, certificated.

b. Zone refined.

c. According to supplier's typical emission spectrographic analysis.

B. Surface Preparation

All rods were first longitudinally milled flat on two sides with a resulting face width of 1.125 inches in order to fit into the specimen holder. Four specimens of 0.25 inch thickness each were cut from each rod. For each metal, one specimen was first polished by using metallographic methods to test the effectiveness of the polishing procedure. If

the specimen surface thus prepared was smooth and bright, the remaining three specimens were prepared by using the same procedure. The procedure used was as follows.

Specimens of 0.25 inch thickness were cut off from the rods with a Felker (Torrance, California) Di-Met Model 11R cut-off machine. A resinoid bonded, metal oxide cut-off wheel, A70-R8-B1, 8 inch diameter and 0.0625 inch thick, was used for the nickel rod and a Electrolon Silico carbide cut-off wheel, C80-010-B1, 8 inch diameter and 0.1875 inch thick, was used for both the copper and zinc rods. Different cutting techniques were required as nickel has a Brinell hardness, soft condition (500 kg), of 70 while that for copper and zinc are 30 and 35, respectively. The cut-off wheels are manufactured by Simonds Abrasive Company, Philadelphia, Pennsylvania and were operated at 3600 rpm. Sufficient cooling water was used during the cutting to prevent any heat tempering to avoid alteration of the microstructure and hardness of the specimen. During cutting, a reasonable amount of wheel pressure was used so the abrasive grains would "bite" and remove the metal in fine chips, and at the same time, cause the wheel bond to break down and present new abrasive particles to the cutting surface.

The metallographic polishing consists of coarse and fine grindings, rough polishing, and final polishing. Nos. 240, 320, 400, and 600 grit silicon carbide papers were used, and water was provided during the coarse and fine grinding

processes. Each step was concluded when the surface appeared uniformly dull over its entire area using visual examination.

Rough polishing was performed by placing the specimen on a nylon cloth over the polishing wheel with 6μ Buehler Metadi diamond as the polishing compound and Buehler No. 60-3250 AB lapping oil as the cooling liquid. The aim of this stage was to eliminate any disturbed surface layers and to prepare an overall surface flatness. After polishing, the specimen was washed first with trichloroethylene, then with ethanol, and finally with tap water.

Gamma form of aluminum oxide with distilled water was used on the Buehler microcloth for the final polishing stage. Microcloth is a napped cloth which is compressible and tends to conform to the surface even under the slightest pressure, The cloth action coupled with the abrasive action has a greater removal rate on the softer phases than on the harder phases.

C. Surface Examination

The requirements of the surface preparation are that the resulting surface should be flat to minimize the error arising from spatial sensitivity of the detector and smooth to reduce the diffuse component which gives rise to experimental error.

Great care has been taken during the grinding and polishing processes in order to prepare a flat surface on the

specimen. Those specimens with good edge preservation were assumed to be sufficiently flat and were selected for the reflectivity measurements.

If the surface is rough, the reflected flux from the specimen which is within the viewing solid angle of the detection system is reduced by virtue of a larger hemispherical diffuse component. The effect of roughness is to redistribute the reflected flux so that the rough surface has an increased diffuse component in addition to the predominant specular component. For the roughness range being considered here, the effect is one of redistributing the flux and not increasing the absorptivity (2).

The normal spectral reflectivity is a very sensitive indicator of roughness when the wavelength is much larger compared with the roughness. The relation is given as

$$R/R_o = \exp[-(4\pi\sigma)^2/\lambda^2]$$

where R is the specular reflectance of the rough surface with surface roughness σ and R_o that of a perfectly smooth surface of the same material. From this relation the error caused by surface roughness in reflectance measurement was estimated (2). For the wavelength range of this experiment, the surface roughness should be less than about 0.02 micron in order to give less than 0.1% error in reflectance. The final stage of polishing of this experiment was performed by using gamma alumina slurry which has particle size of 0.05 micron. Thus, the requirement can be reasonably

achieved.

In this range of roughness, the conventional technique such as mechanical profilometer is inaccurate and it is also destructive to the surface measured. The surface roughness can be examined by using the Thermal Comparator*. The Thermal Comparator, a tool for rapid measurement of thermal conductivity, is also quite useful for examination of surface characteristics and for qualitative determinations of film thickness, roughness, oxidation, etc.

The Thermal Comparator consists of a thermocouple mounted very close to the surface of a fine pointed probe which in turn is mounted in a large heat source maintained at some excess temperature (15-30^{o}C) above the ambient. When the probe is touched to a specimen surface, the tip at which the thermocouple (differentially connected with the main source) is located, quickly reaches an intermediate temperature between ambient and that of the source. If the specimen is a smooth, homogeneous solid, the ratio of the thermocouple EMF from the specimen when compared to a similarly prepared surface of a standard reference material will yield the thermal conductivity. If the surfaces are roughened, the point probe will contact the asperities rather than the full surface resulting in a lower EMF response and hence giving a qualitative measure of roughness. The Thermal Comparator can

*Manufactured by the Technometrics, Inc., West Lafayette, Indiana.

also be used to rapidly determine the similarity of surface preparation for a collection of specimens before reflectance measurements.

To determine the influence of the polishing technique on roughness, measurements of the Thermal Comparator response were made following the various stages of polishing. Polishing continued until all specimens indicated the same EMF (qualitatively having the same minimum roughness).

Zinc specimens were purposely prepared with different resulting surface roughness. The results of the reflectivity measurement and the Thermal Comparator EMF response of each specimen are shown in Figure 19. As reasoned above, the zinc specimen (No.2) with highest EMF response gives the highest reflectivity.

From the reflectivity data given in Figure 19, the surface roughness of specimens Nos. 1 and 3 (assuming specimen No. 2 as a reference) by using the relation of the reflectance and roughness, at four and eight microns, gave the roughness value as 0.02-0.04 micron for specimen No. 1 and 0.06-0.10 micron for specimen No. 3.

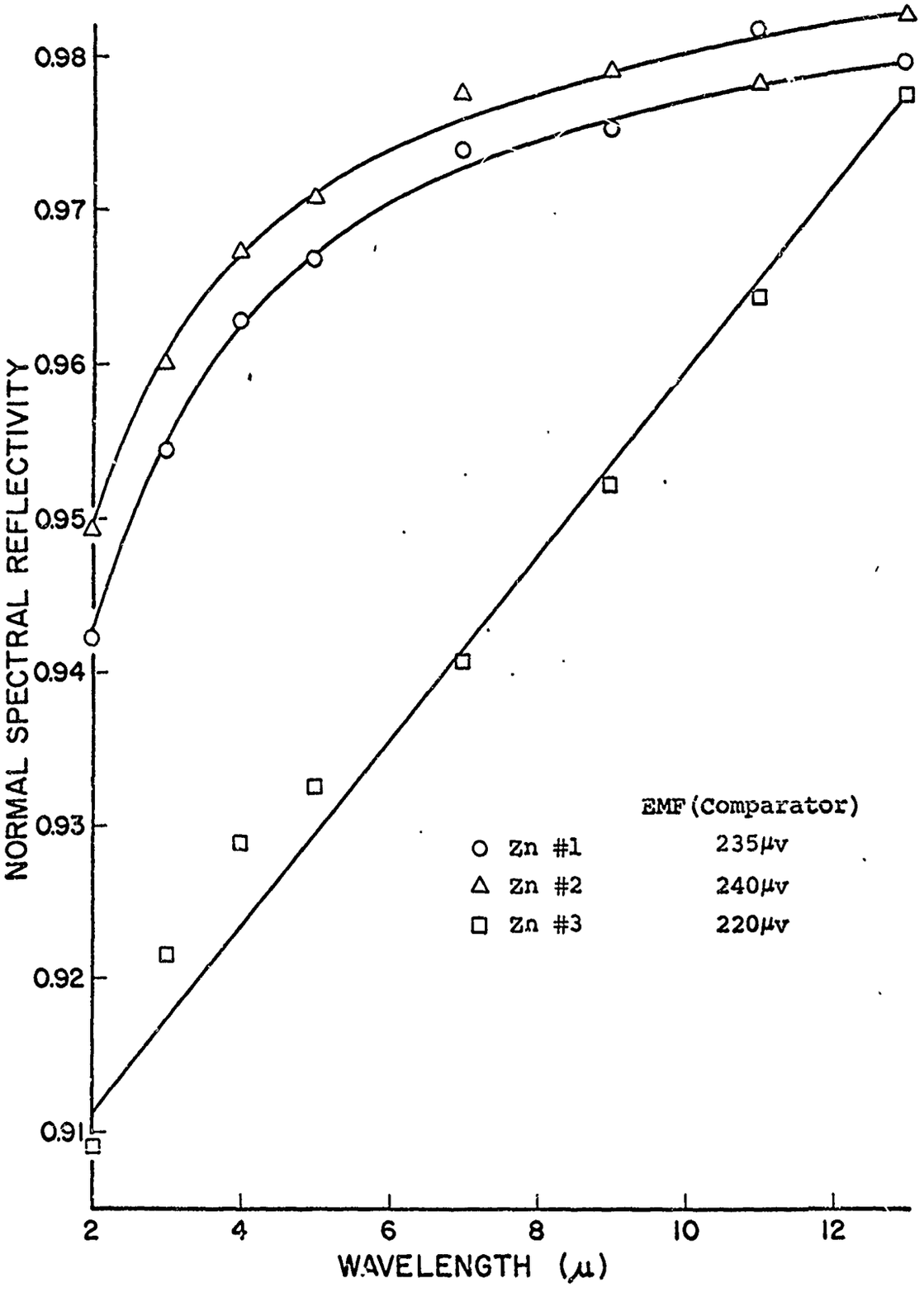

Figure 19. Normal Spectral Reflectivity of Zinc as a Function of Surface Preparation.

X. EXPERIMENTAL RESULTS AND THEIR COMPARISON WITH THEORY

Measurements of normal spectral reflectivity were made on metallographically polished copper, zinc, and nickel, and aged, high vacuum evaporated aluminum specimens. Three specimens for each polished material, which visual examination showed good edge preservation, were selected for the measurement. Figures 20, 23, and 26 show the measurement results of copper, zinc, and nickel. The comparison between the present data and literature values are presented in Figures 21,24, and 27. Data on evaporated aluminum and their comparison with that of Bennett' have been shown in Figure 18 in the previous chapter. The comparisons of measurements and the predictions of theoretical models are given in Figures 22,25,28, and 29. They are plotted as absorptivity, i.e., 1-R, vs wavelength in full logarithmic coordinates. The physical parameters used for the theoretical calculations are listed in Table 7.

Copper - Average reflectivity values of specimen Nos. 1, 2, and 4 are plotted in Figure 20. Generally, deviations of the experimental data from a smooth curve are rather small. The scattering of data at three and five microns is due to the atmosphere absorption giving rise to a higher noise level of the output signal and higher uncertainty. The present

Table 7. Physical Parameters Used for Theoretical Calculations(300°K).

	ω_o	$\gamma_{ep}(\alpha)b_{ep}(\alpha)$	$\frac{1}{\Omega_{ee}}$	N^{**}	$\sigma_o{}^{*}$	References
	$(sec)^{-1}$	$(sec)^{-1}$	(sec)	(Cm^{-3})	(Cgs esu)	
Al	15×10^{15}	137×10^{12}	0.8×10^{-16}	6×10^{22}	3.2×10^{17}	(1),(26),(36),(54)
Cu	12.25×10^{15}	62.1×10^{12}	0.7×10^{-16}	8.5×10^{17}	5.3×10^{17}	(36),(38),(48),(54)
Zn	6.8×10^{15}	72.3×10^{12}	2.35×10^{-16}	6.6×10^{22}	1.52×10^{17}	(30),(36),(54)
Ni				9.14×10^{22}	1.315×10^{17}	(36),(54)

*Also used for Hagen-Rubens Equations.
**Based on one conduction electron per atom.

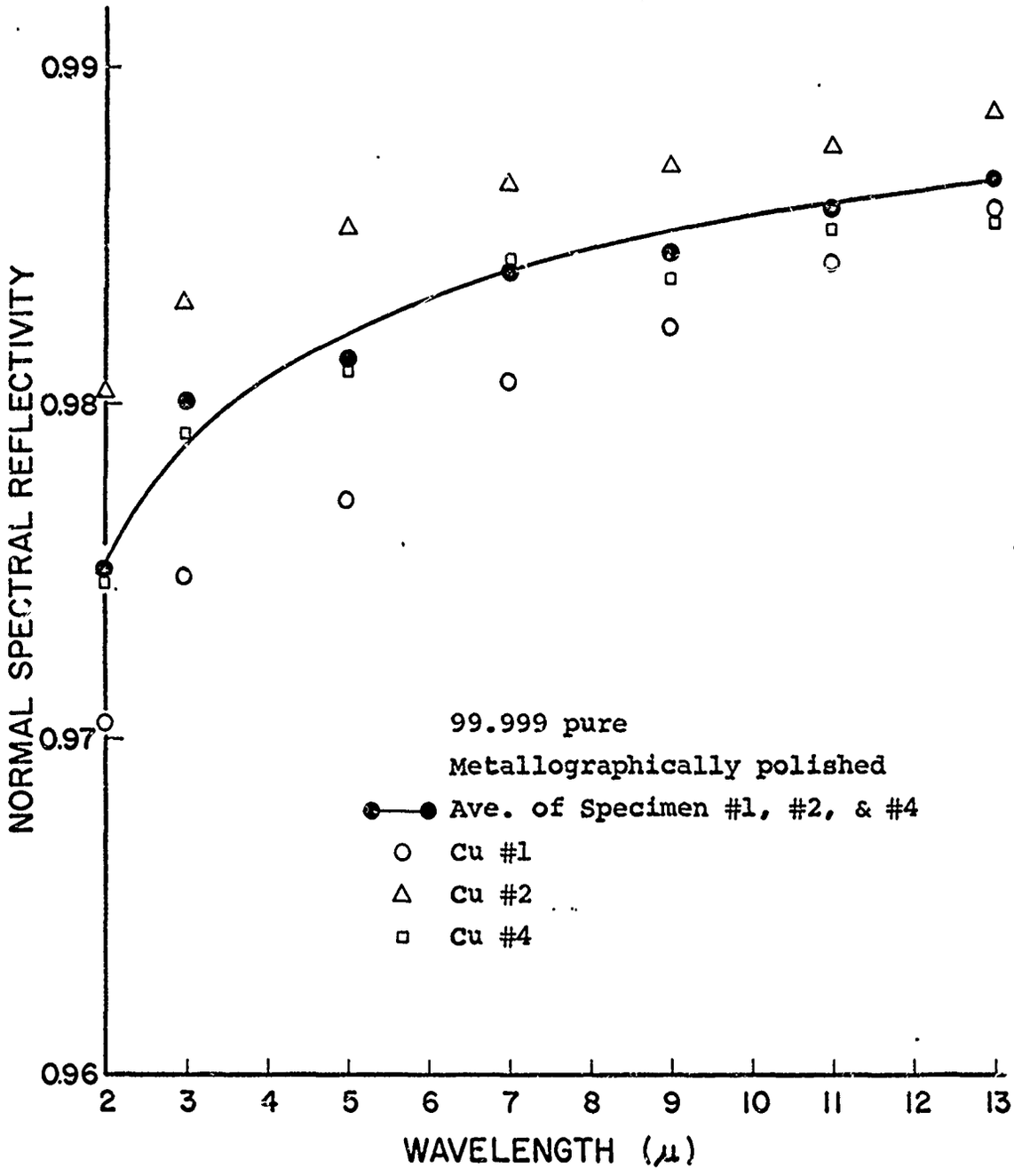

Figure 20. Normal Spectral Reflectivity of Copper.

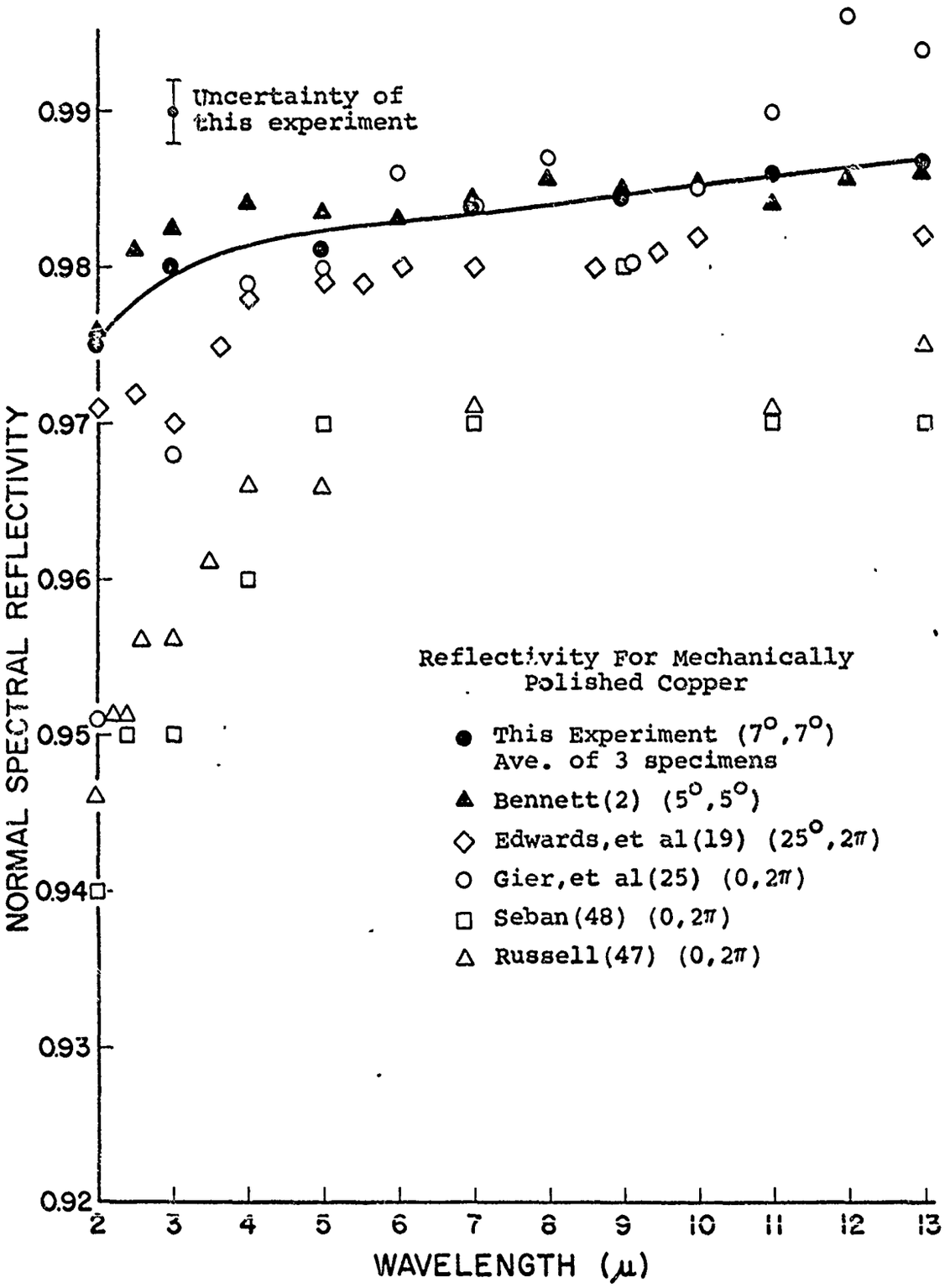

Figure 21. Normal Spectral Reflectivity of Copper and Its Comparison With Published Values.

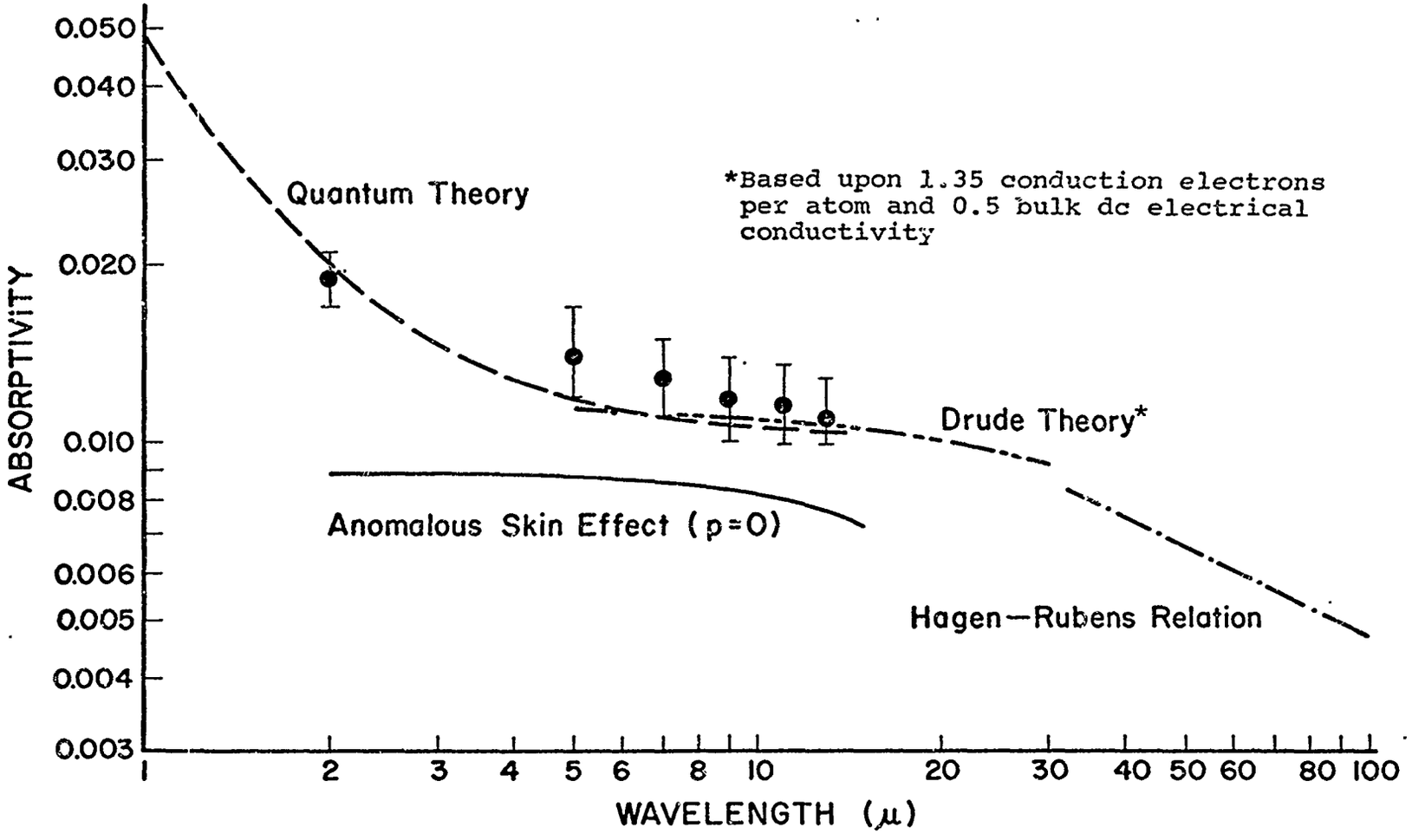

Figure 22. Absorptivity of Copper and Its Comparison With Theory.

results are comparable with Bennett's values (Figure 21).

Theoretical predictions and their comparison with experimental data are presented in Figure 22. Prediction of absorptivity using the theory of anomalous skin effect has been made. When diffuse electronic reflection, one conduction electron per atom, and bulk dc conductivity are assumed, the prediction is lower than the present data. No further attempt was made to fit the experimental data with the theoretical equation derived from the theory of anomalous skin effect. The predicted curve by using quantum theory is within the uncertainty of the experimental values. Absorptivity calculated by using Hagen-Rubens relation is presented to show the trend expected toward long wavelengths. Assuming 1.35 conduction electrons per atom (from Hall effect measurement)(34), the simple Drude theory (4) yields that,with 0.5 bulk dc electrical conductivity, best agreement can be obtained between the experimental data and the theoretical prediction at 13 microns. These two parameters are used to predict the absorptivity from 5 microns to longer wavelengths. The reason for the discrepancy between theory and experimental values at the shorter wavelength end is because in the neighborhood of the absorption edge and at higher frequencies, the damping coefficient, which is assumed to be constant, becomes frequency dependent (4).

Zinc - Data of specimen No. 2 are presented in Figure 23. Specimen No. 2 has the most smooth surface among three specimens prepared. The experimental curve is very smooth

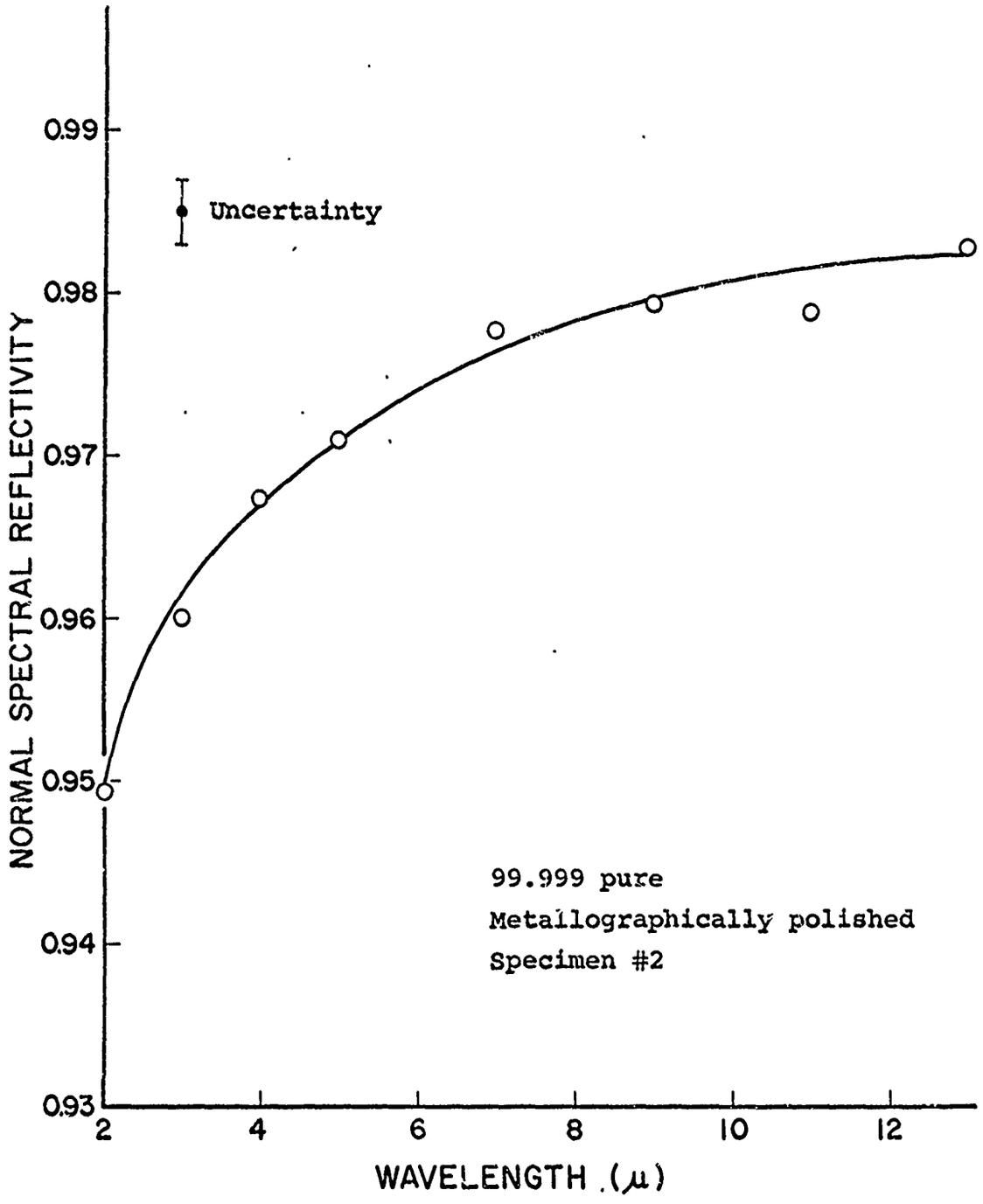

Figure 23. Normal Spectral Reflectivity of Zinc.

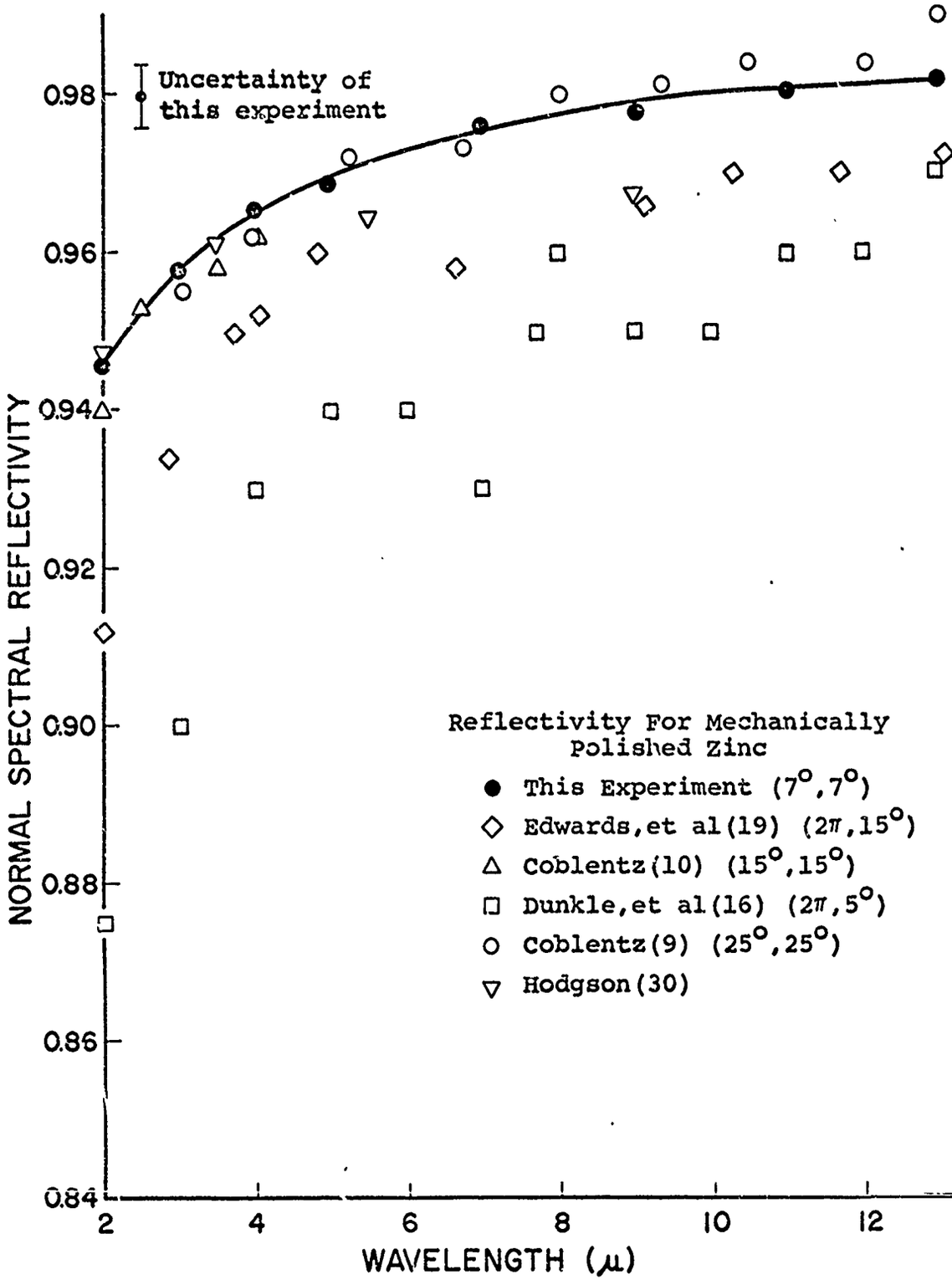

Figure 24. Normal Spectral Reflectivity of Zinc and Its Comparison With Published Values.

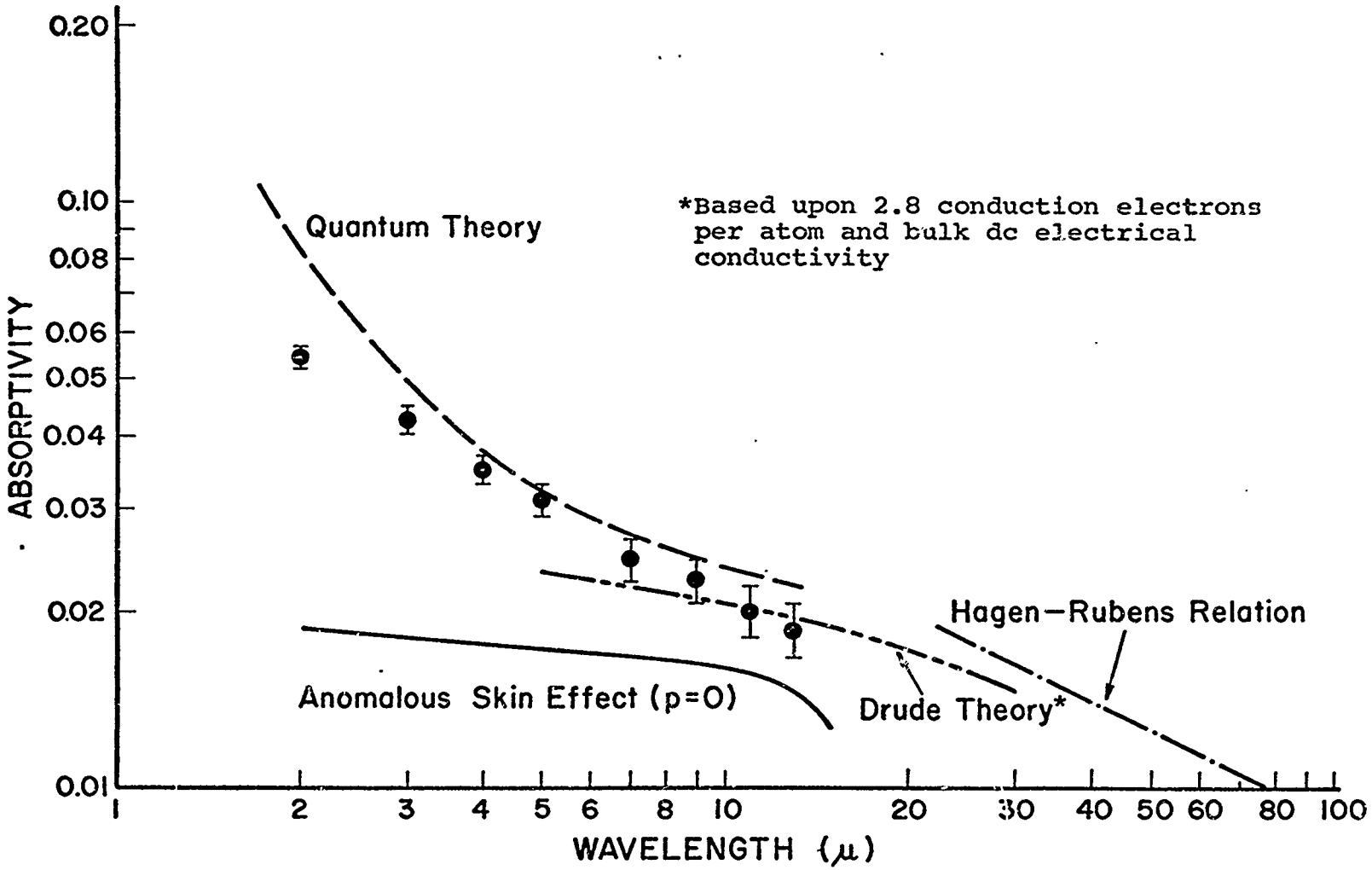

Figure 25. Absorptivity of Zinc and Its Comparison With Theory.

except the lower value at 11 microns which is probably due to the experimental error. When compared with literature values (Figure 24), the present results are among the highest.

Theoretical predictions and their comparison with experimental data are presented in Figure 25. The predictions made by the theory of anomalous skin effect and quantum theory and their comparisons with experimental data are similar to that of the copper specimens. The experimental value has the similar slope with the curve calculated from the Hagen-Rubens relation. Assuming 2.8 conduction electrons per atom (from Hall Effect measurement)(34), the simple Drude theory (4) yields that with bulk dc electrical conductivity, best agreement can be obtained between the experimental data and the theoretical prediction at 13 microns. These two parameters are used to predict the absorptivity from five microns to longer wavelengths.

Nickel - The reflectivity data for the three nickel specimens are shown in Figure 26. Because nickel has a rather high hardness, specimens are easily polished and yield a smooth and bright surface. Nickel surface is not oxidized in air at room temperature. These may explain why the data of all three specimens agree so closely with each other.

Theoretical predictions and their comparison with experimental data are presented in Figures 27 and 28. Prediction of absorptivity using the theory of anomalous skin effect has been made. When diffuse electronic reflection, one conduction

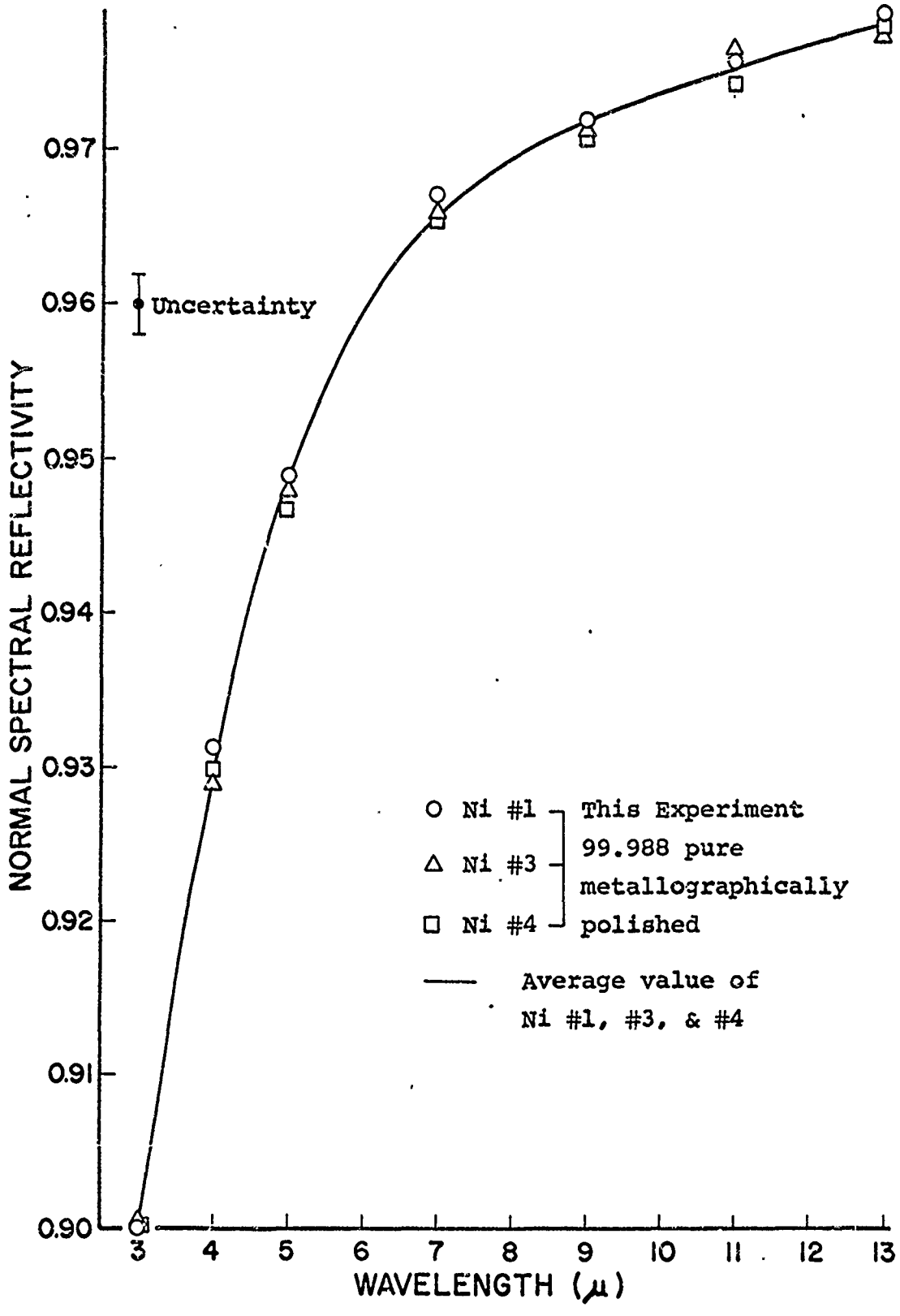

Figure 26. Normal Spectral Reflectivity of Nickel.

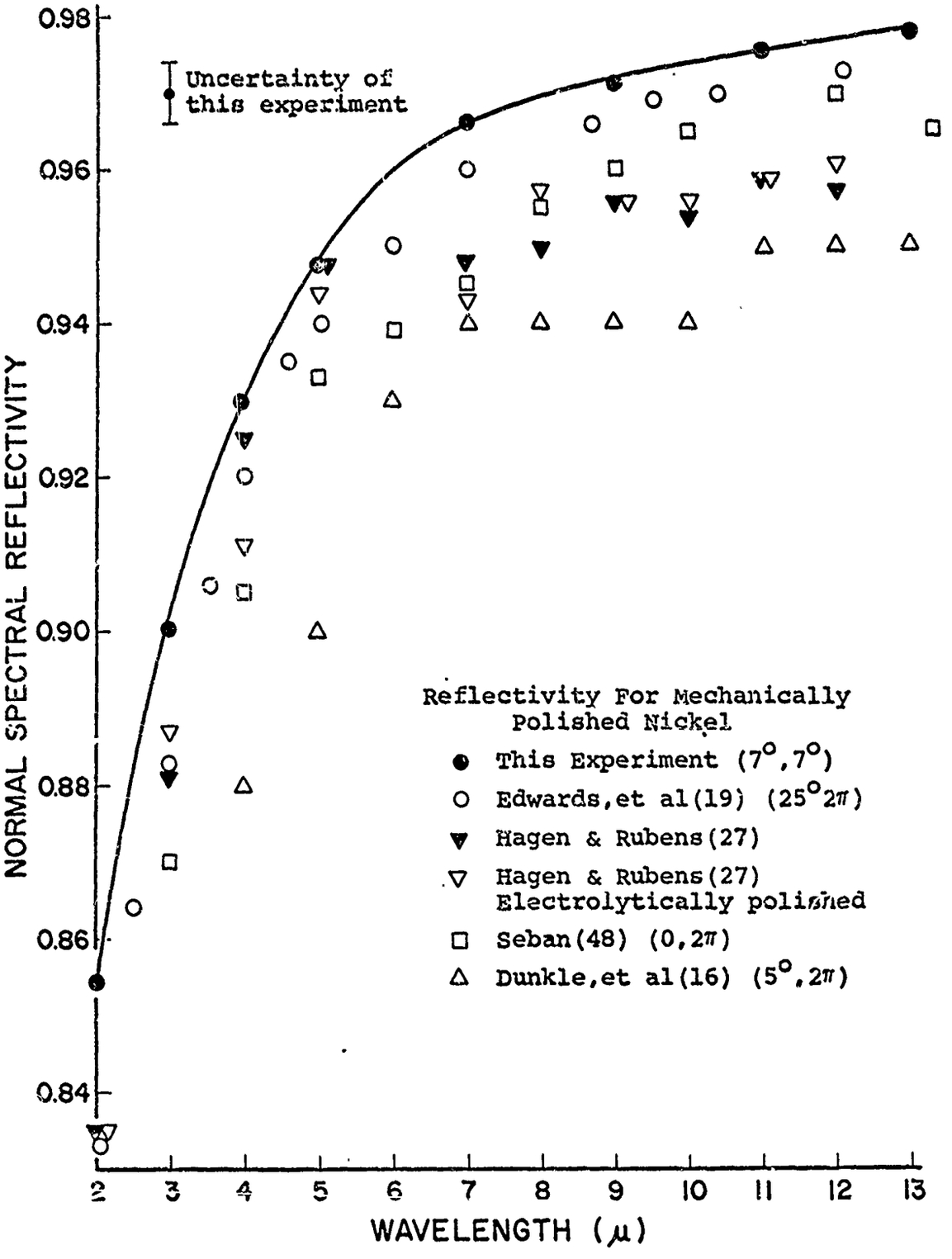

Figure 27. Normal Spectral Reflectivity of Nickel and Its Comparison With Published Values.

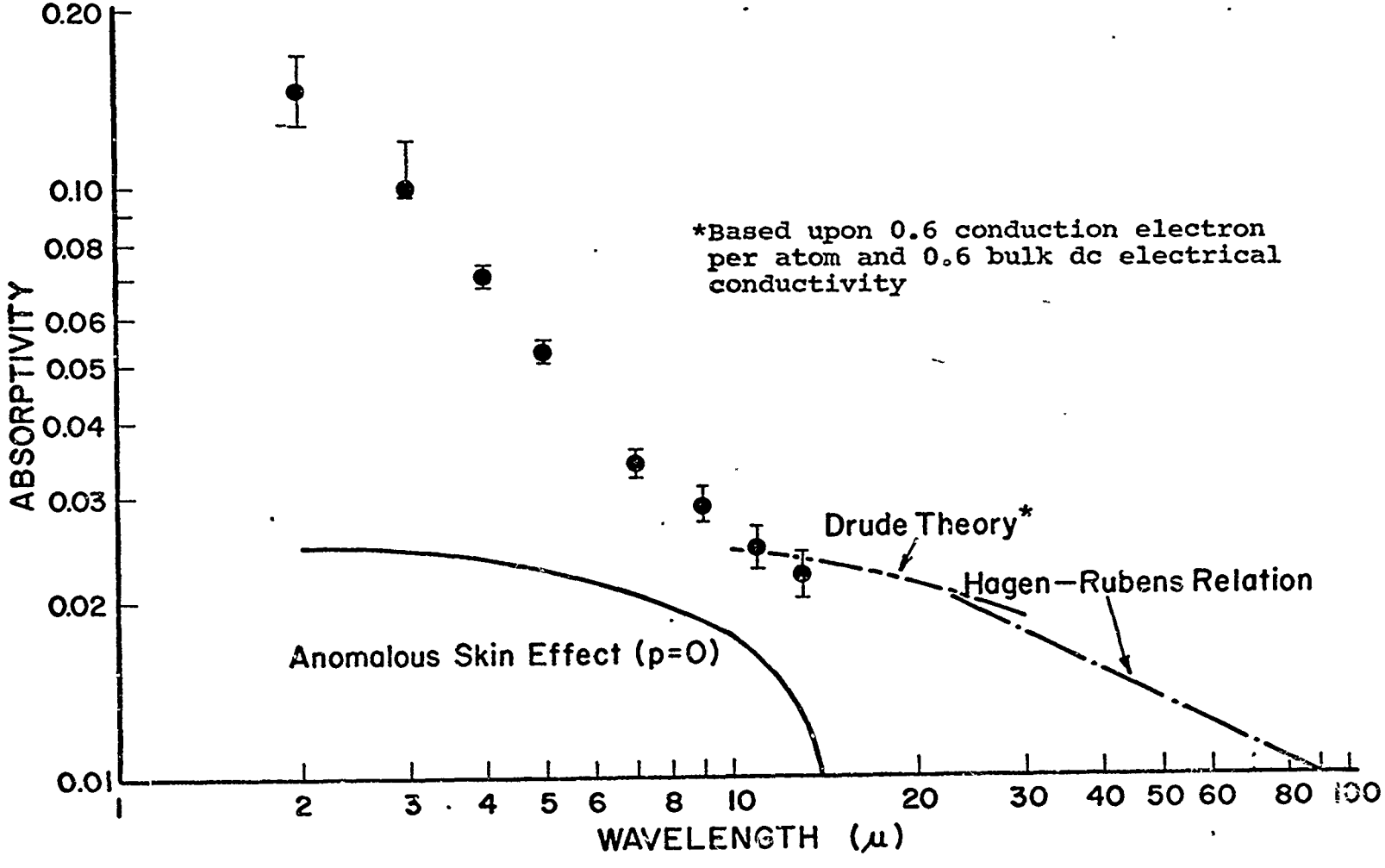

Figure 28. Absorptivity of Nickel And Its Comparison of Theory.

electron per atom, and bulk dc conductivity are assumed, the prediction is lower than the present data. No calculation is made based on quantum theory. Nickel is a ferromagnetic material and it is rather difficult to estimate its physical parameters from the two simple optical constants and wavelength relations. Assuming 0.6 conduction electron per atom (37), the simple Drude theory (4) yields that with 0.6 bulk dc electrical conductivity, best agreement can be obtained between the experimental data and the theoretical prediction at 13 microns. These two parameters are used to predict the absorptivity from about 10 microns to longer wavelengths.

Aluminum - Experimental data on aged, high vacuum evaporated aluminum (Figure 18) are comparable with literature values (5) of specimen prepared under the same condition.

Theoretical predictions and their comparison with experimental data are presented in Figure 29. The predictions made by the theory of anomalous skin effect and quantum theory and their comparisons with experimental data are similar to that of the copper specimens. Absorptivity calculated by using Hagen-Rubens relation is presented to show the trend expected toward long wavelengths. Bennett et al (5) have shown the validity of the Drude theory for ultra-high vacuum evaporated aluminum film in the infrared range. Their calculation was based on bulk dc conductivity and 2.6 conduction electrons per atom of aluminum. Assuming 2.6 conduction electrons per

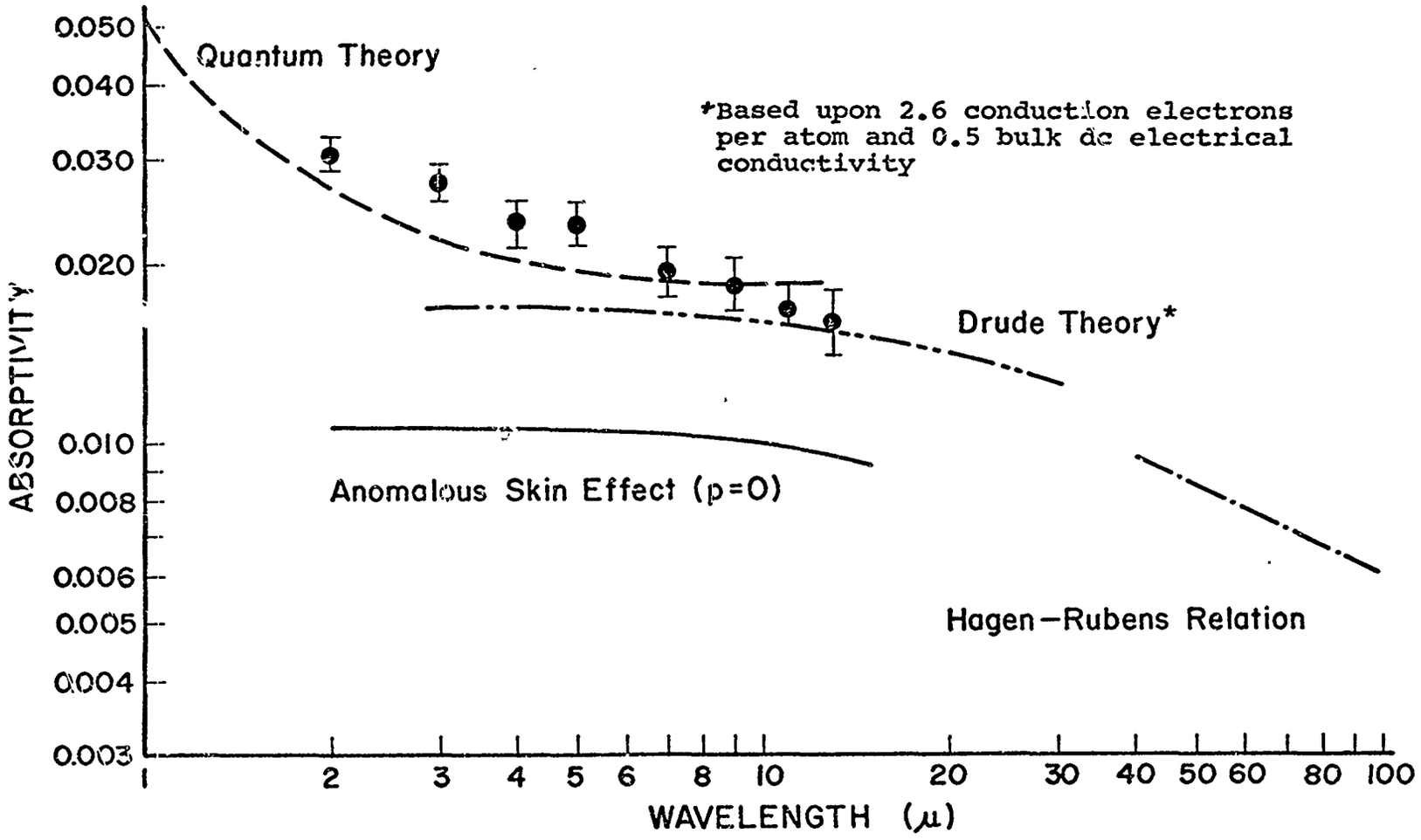

Figure 29. Absorptivity of Aluminum and Its Comparison With Theory.

atom, the simple Drude theory (4) yields that with 0.5 dc electrical conductivity, best agreement can be achieved between the present experimental data and the theoretical prediction at 13 microns. These two parameters are used to predict the absorptivity in the infrared range.

Smooth curves based upon present measurement and theory are drawn for copper, zinc, nickel, and aluminum. They are shown in Figures 30 and 31. Absorptivity data extracted from these smooth curves are presented in Table 8, and are considered as the most probable absorptivity values.

Table 8. Most Probable Absorptivity Values Based Upon Measurement and Theory*

λ (μ)	Absorptivity			
	Cu	Zn	Ni	Al
2	0.0190	0.0560	0.1550	0.0305
4	0.0140	0.0342	0.0600	0.0236
6	0.0126	0.0270	0.0385	0.0210
8	0.0118	0.0235	0.0302	0.0193
10	0.0114	0.0215	0.0260	0.0182
15	0.0107	0.0189	0.0220	0.0161
20	0.0101	0.0175	0.0205	0.0148
25	0.0096	0.0166	0.0192	0.0138
30	0.0092	0.0156	0.0180	0.0130
35	0.0087	0.0147	0.0172	0.0122
40	0.0083	0.0140	0.0164	0.0115
50	0.0073	0.0128	0.0150	0.0105
60	0.0068	0.0118	0.0140	0.0096
70	0.0062	0.0110	0.0132	0.0090
80	0.0058	0.0103	0.0124	0.0084
90	0.0054	0.0098	0.0117	0.0079
100	0.0051	0.0093	0.0111	0.0074

*Preliminary estimate; uncertainty $\pm$0.002 unit.

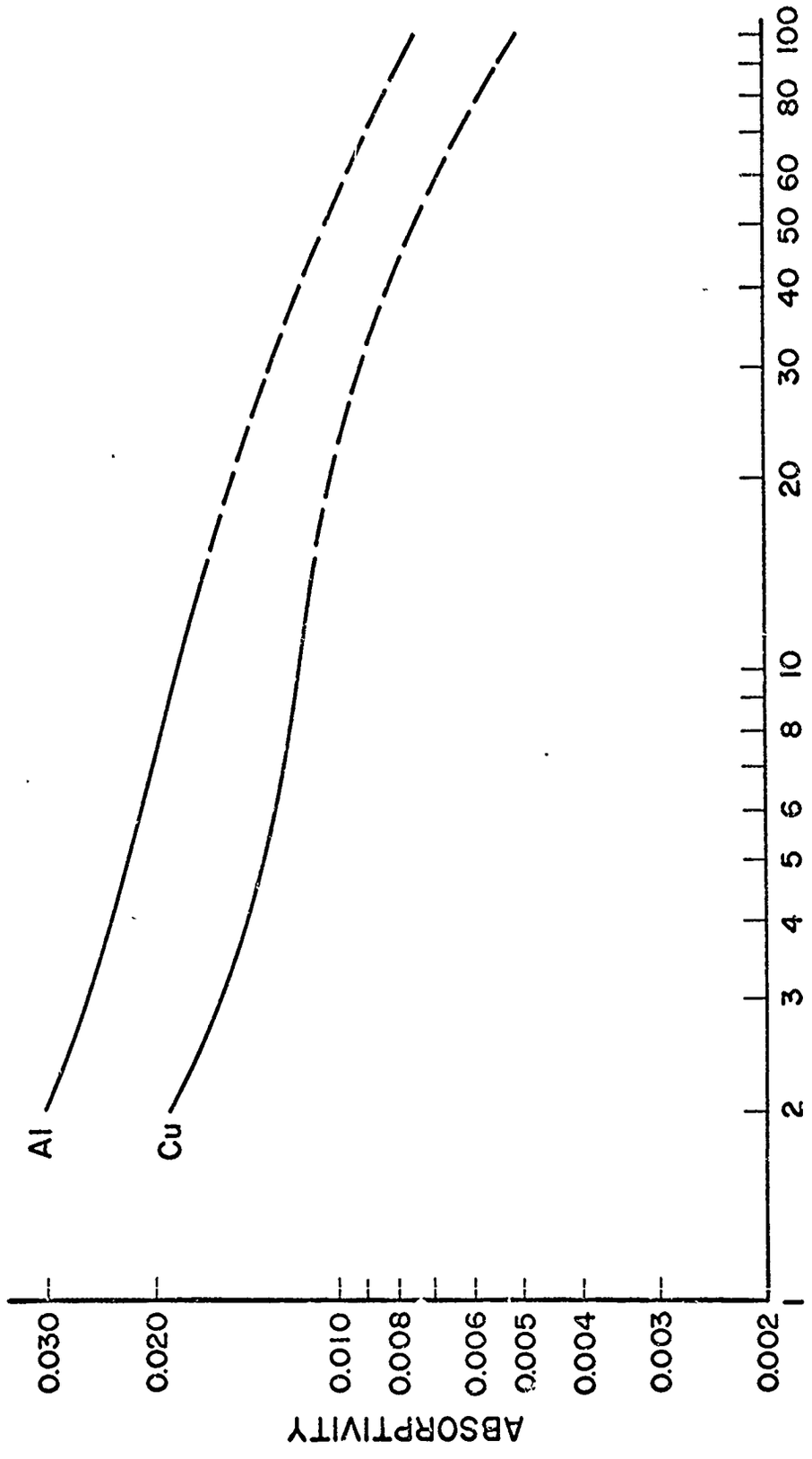

Figure 30. Most Probable Absorptivity Curves of Cu and Al Based Upon Measurement and Theory.

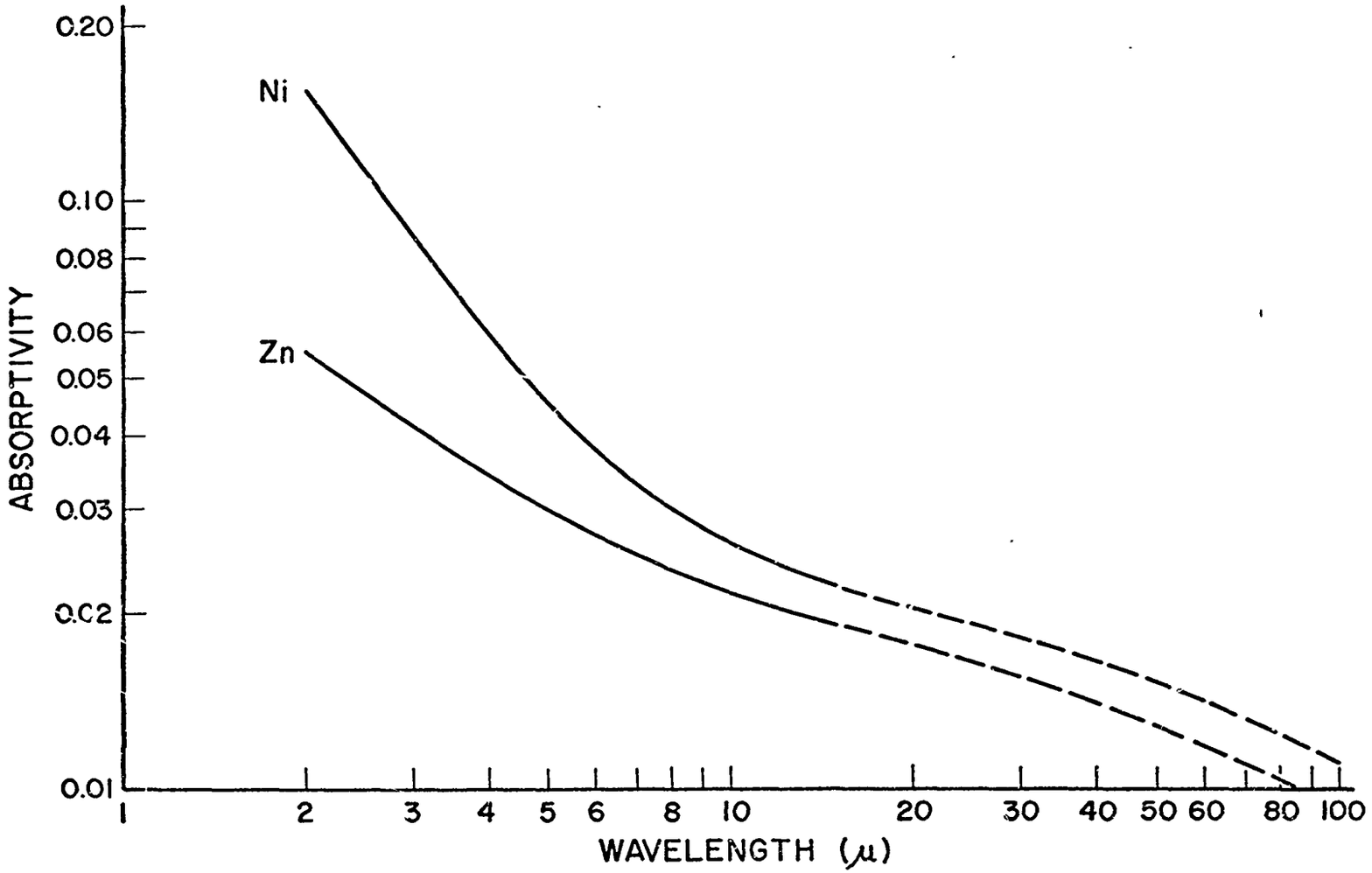

Figure 31. Most Probable Absorptivity Curves of Zn and Ni Based Upon Measurement and Theory.

XI. SUMMARY AND CONCLUSIONS

An apparatus was fabricated to measure normal spectral reflectivity. The multiple reflection technique utilized in this investigation allows the reflectivity measurement of infrared radiation to have the accuracy of about ± 0.002 reflectivity unit.

Measurements of normal spectral reflectivity were made on the pure metallic elements: metallographically polished copper, zinc, and nickel and aged, high vacuum deposited aluminum. Special attention was given to the performance evaluation of the reflectometer and bulk specimen preparation.

The theoretical portion of this study has included the review of the theoretical models in the free-electron frequency range and their applicability. It has been found that absorptivity predicted by the theory of anomalous skin effect, assuming diffuse electronic reflection, one conduction electron per atom and bulk conductivity, is lower than that of the present experiment. No attempts were made to fit the data using this theory. On the other hand, it is seen that the prediction made by simple quantum theory fits well with the experimental results. Simple Drude Theory and Hagen-Rubens relation were used to predict absorptivity

values in the longer wavelength range not measured in this experiment. Most probable absorptivity values of copper, zinc, nickel, and aluminum from two to 100 microns were obtained, based on measurement and theory.

XII. LIST OF REFERENCES

XII. LIST OF REFERENCES

1. Beattie, J. R., Optical Constants of Metals in the Infra-red-Experimental Methods. Phil. Mag., 46(7), 235-45,1955.

2. Bennett, H. E., Influence of Surface Roughness, Surface Damage, and Oxide Films on Emittance. Symposium on Thermal Radiation of Solids, NASA SP-55, 145-52, 1965.

3. Bennett, H. E., Accurate Method for Determining Photometric Linearity. Appl. Opt., 5(8), 1265-70, 1966.

4. Bennett, H. E. and Bennett, J. M., Validity of the Drude Theory for Silver, Gold and Aluminum in the Infrared. Proceedings of the Intern. Colloq. held in Paris (1965), 174-88, North-Holland, 1966.

5. Bennett, H. E., Bennett, J. M., and Ashley, E. J., Infrared Reflectance of Evaporated Aluminum Films. J. Opt. Soc. Am., 52(11), 1245-50, 1962.

6. Bennett, H. E. and Koehler, W. F., Precision Measurement of Absolute Specular Reflectance with Minimized Systematic Errors. J. Opt. Soc. Am., 50(1), 1-6, 1960.

7. Biondi, M. A., Optical Absorption of Copper and Silver at 4.2°K. Phys. Rev., 102(4), 964-7, 1956.

8. Brandenberg, W. M., Clausen, O. W., and McKeown, D., High Precision Method for Measuring the Absorptance of Evaporated Metals. J. Opt. Soc. Am., 56(1), 80-6, 1966.

9. Coblentz, W. W., Radiometric Investigations of Infra-red Absorption and Reflection Spectra. NBS Bull., 2, 457-78, 1906.

10. Coblentz, W. W., Reflecting Power of Monel Metal, Stellite, and Zinc. NBS Bull., 16, 249-52, 1920.

11. Conn, G. K. T. and Avery, D. G., Infrared Methods.,131, Academic Press, 1960.

12. DeWitt, D. P., The Effect of Surface Roughness on the Normal Spectral Emissivity of Tungsten. Ph.D. Thesis, Purdue Univ., 1963.

13. Dickson, P. F. and Jones, M. C., Infrared Reflectances of Metals at Cryogenic Temperatures - A Compilation from the Literature. NBS Tech. Note 348, 1-60, 1966.

14. Dingle, R. B., The Anomalous Skin Effect and the Reflectivity of Metals. I. Theory. Physica, 19, 311-47, 1953.

15. Dingle, R. B., The Anomalous Skin Effect and the Reflectivity of Metals. II. Comparison Between Theoretical and Experimental Optical Properties. Physica, 19, 348-64, 1953.

16. Dunkle, R. V. and Gier, S. T., Progress Report for the Year Ending June 27, 1952. 1-73, Calif. Univ. Inst. of Eng. Research, Berkeley (AD 16830), 1953.

17. Dunn, S. T., Design and Analysis of An Ellipsoidal Mirror Reflectometer. Ph. D. Thesis, Oklahoma State University, 1965.

18. Dunn, S. T., Flux Averaging Devices for the Infrared. NBS Tech. Note 279, 1965.

19. Edwards, D. K. and deVolo, N. B., Useful Approximations for the Spectral and Total Emissivity of Smooth Bare Metals. 174-88, Advances in Thermophysical Properties at Extreme Temperatures and Pressures, ASME, 1965.

20. Fowler, P., Far Infrared Absorptance of Gold. M. S. Thesis, MIT (AD 418456), 1-57, 1960.

21. Garbuny, M., Optical Physics. Academic Press, 1965.

22. Gates, D. M., Shaw, C. C., and Beaumont, D., Infrared Reflectance of Evaporated Metal Films. J. Opt. Soc. Am., 48(2), 88-9, 1958.

23. Gibson, K. S., Spectrophotometry (200 to 1000 Millimicrons). NBS Circular 484, 1-48, 1949.

24. Gier, J. T., Dunkle, R. V., and Bevans, J. T., Measurement of Absolute Spectral Reflectivity From 1.0 to 15 Microns. J. Opt. Soc. Am., 44(4), 558-62, 1954.

25. Gier, J. T., Possner, L., Test, A. J., Dunkle, R. V., and Bevans, J. T., The Absolute Spectral Reflectivity of Certain Pigments and Metals in the Wavelength Range Between 2 and 16 Microns. DDC and CFSTI NR-015-202 ATI-59635, 1-4, 1949.

26. Golovashkin, A. I., Motulevich, G. P., and Shubin, A.A., Determination of Microscopic Parameters of Aluminum From Its Optical Constants and Electric Conductivity. Soviet Phys. JETP, 11(1), 38-41, 1960.

27. Hagen, E. and Rubens, H., The Relations of the Reflectivity and the Emissivity of Metals to Their Electrical Conductivity. Ann. Physik. 11(8b), 873-901, 1903.

28. Harrison, W. N., Richmond, J. C., Ahorten, F. J., and Joseph, H. S., Standardization of Thermal Emittance Measurements, Part 4: Normal Spectral Emittance 800-1400 K. NBS, WADC TR59-510, 16-20, 1962.

29. Hass, G., American Institute of Physics Handbook. 6=119, 2nd Edition, McGraw-Hill, 1963.

30. Hodgson, J. N., The Infra-red Properties of Some Metallic Films. Proc. Phys. Soc., B68(9), 593-602, 1955.

31. Holstein, T., The Theory of Optical and Infrared Properties of Metals. NASA TND-1523, 1-253, 1963.

32. Jacques, J. A. and Kuppenheim, H. F., Theory of the Integrating Sphere. J. Opt. Soc. Am., 45(6), 460-70, 1955.

33. Jenkins, F. A. and White , H. E., Fundamentals of Optics. 302-465, 3rd Edition, McGraw-Hill, 1957.

34. Kittel, C., Quantum Theory of Solids. 105, John Wiley & Sons, 1966.

35. Kline, S. J. and McClintock, F. A., Describing Uncertainties in Single-Sample Experiments. Mech. Eng., 75, 3-8, 1953.

36. Meaden, G. T., Electrical Resistance of Metals, Plenum Press, 1965.

37. Mott, N. F. and Jones, H., The Theory of the Properties of Metals and Alloys, 262, Dover, 1958.

38. Padalka, V. G. and Shklyarevskii, I. N., Determination of the Microcharacteristics of Cu From Its Infrared Optical Constants and Its Conductivity At 82°K and 295°K. Opt. & Spectro., 12(2), 158-62, 1961.

39. Perkin-Elmer Corporation, Instruction Manual for Infrared Equipment. 3A, 52, Perkin-Elmer Corporation, 1956.

40. Perkin-Elmer Corporation, Instruction Manual Vol. I., Introduction To Infrared Spectrometry, 11 & 12, Perkin-Elmer 990-9000, 1952.

41. Plyler, E. K., Blaine, L. R., Nowak, M., Reference Wavelengths for Calibrating Prism Spectrometers. J. Res. NBS, 58(4), 193-200, 1957.

42. Reitz, J. R. and Milford, F. J., Foundations of Electromagnetic Theory, 194, 294-317, Addison-Wesley, 1962.

43. Richmond, J. C., Dunn, S. T., DeWitt, D. P., and Hayes, W. D. Jr., Procedures For Precise Determination of Thermal Radiation Properties, November 1963 to October 1964., NBS Tech. Note 267, 37-40, 1965.

44. Roberts, S., Interpretation of the Optical Properties of Metal Surfaces. Phys. Rev., 100(6), 1667, 1956.

45. Roberts, S., Optical Properties of Nickel and Tungsten and Their Interpretation According to Drude's Formula, Phys. Rev., 114, 104-115, 1959.

46. Roberts, S., Optical Properties of Copper, Phys. Rev. 118(6), 1509-18, 1960.

47. Russell, D. A., Spectral Reflectance of Rough Surfaces in the Infrared. M.S. Thesis, Univ. of Calif. at Berkeley, 1-47, 1961.

48. Seban, R. A., The Emissivity of Transition Metals in the Infrared. J. Heat Transfer, Trans., ASME, C87(2), 173-6, 1965.

49. Shklyarevskii, I. N. and Padalka, V. G., Measurements of the Optical Constants of Copper, Gold, and Nickel in the Infrared Region of the Spectrum. Opt. & Spectr., 6(1), 45-8, 1959.

50. Shklyarevskii, I. N. and Padalka, V. G., The Anomalous Skin-Effect and Optical Constants of Copper, Gold, and Nickel in the Infrared Region of the Spectrum, Opt. & Spectr., 6(6), 505-7, 1959.

51. Sokolov, A. V., Optical Properties of Metals. 1-472, American Elsevier, 1967.

52. Strong, J. L., Procedures in Experimental Physics. 376, Prentice Hall, 1938.

53. Twidle, G. G., The Spectral Reflectivity of Back-Surface and Front-Surface Aluminized Mirrors. Brit. J. Appl. Phys., 8, 337-9, 1957.

54. Weast, R. C. (Editor), Handbook of Chemistry and Physics, 47th ed., Chemical Rubber Co., 1966.

55. Zipin, R. B., The Directional Spectral Reflectance of Well-Characterized Symmetric V-Grooved Surfaces. Ph.D. Thesis, Purdue Univ. 1965.

APPENDIXES

APPENDIX A

MONOCHROMATOR SLIT WIDTH LINEARITY

In a single pass monochromator, the radiation beam, after passing through the entrance slit, goes through the "collimator" to the prism and then from the prism to the "telescope" and to the exit slit. (see Figure A-1).

The spectral range of radiation falling on the exit slit of width ΔX_2 in the focal plane of the "telescope" is:

$$\Delta \lambda = \frac{\Delta \lambda}{\Delta \theta} \cdot \Delta \theta \cong \left(\frac{d \lambda}{d \theta}\right) \frac{\Delta X2}{f_2} \qquad \text{(A-1)}$$

The radiant flux, B, accepted by an entrance slit with ΔX_1 and height ℓ is such that

$$B \simeq \left(\Delta X_1 \cdot \ell\right)\left[\left(E_\lambda \cdot \Delta \lambda\right) \frac{D^2}{f_1^2}\right] \qquad \text{(A-2)}$$

Where $E_\lambda \cdot \Delta\lambda$ is the power emitted by the source per unit area per unit solid angle in the wavelength range λ to $\lambda+\Delta \lambda$. Aberrations of mirrors and curvature of the spectral images are second order effects and may be safely ignored; losses by reflection polarization and absorption are neglected here.

Inserting (A-1) into (A-2) and setting $f_1=f_2=f$ and $\Delta X_1 = \Delta X_2 = s$ conditions for the P-E Model 98 monochromator, yield

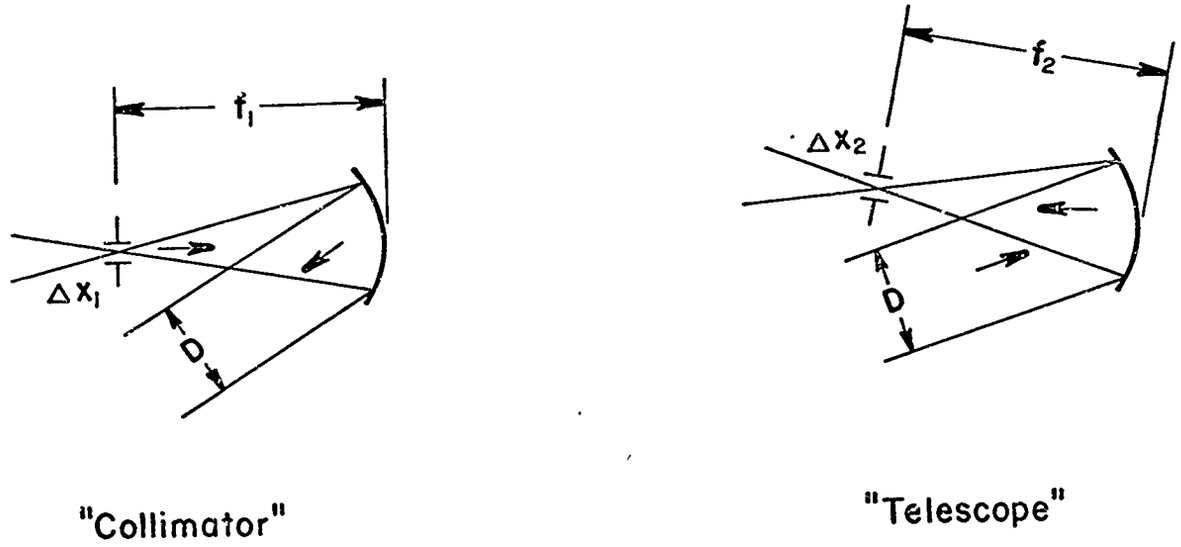

"Collimator" "Telescope"

Figure A-1. "Collimator" and "Telescope" of Monochromator Optics.

$$B \simeq \left[\frac{\ell_D{}^3}{f^3} E_\lambda \left(d\lambda/d\theta\right)\right](s)^2 \qquad \text{(A-3)}$$

The parameters ℓ, D, and f are fixed values; E_λ and $(d\lambda/d\theta)$ are constant for a given wavelength. Therefore, for a given wavelength the radiative energy emerging from the exit slit is proportional to the square of the slit width setting. Note that Equation (A-3) was derived by neglecting diffraction.

APPENDIX B

DETERMINATION OF RESOLVED BAND WIDTH (OR SPECTRAL SLIT WIDTH) OF THE MONOCHROMATOR

The resolved band width, $\Delta\lambda$, of a monochromator is defined as half of the total wavelength interval falling on the exit slit; it is a measure of the wavelength purity of the beam emerging from the exit slit. It is necessary to know the resolved band width as a function of slit width and wavelength. This function will aid the choosing of proper slit widths at different wavelengths for reflectivity measurements. These slit width settings will give minimum error due to the effect of slit opening and still allow enough energy for detection (23).

The resolved band width can be written as

$$\Delta\lambda = (\Delta\lambda)_d + (\Delta\lambda)_p \qquad (A-4)$$

The first term $(\Delta\lambda)_d$ is due to the dispersion of the prism and the second term $(\Delta\lambda)_p$ is the Rayleigh term and results from the diffraction pattern of an infinitely narrow slit. Both terms will be derived in detail.

Determination of $(\Delta\lambda)_d$ - The spectral range of radiation going through the prism once and falling on the exit slit of width s in the focal plane is (11)

$$(\Delta\lambda)_d = \frac{(\Delta\lambda)_d}{\Delta\theta} \cdot \Delta\theta = \left(\frac{d\lambda}{d\theta}\right)_d \frac{s}{f} \qquad \text{(A-5)}$$

which can be written as

$$(\Delta\lambda)_d = \frac{1}{\left(\frac{d\theta}{dn}\right)\left(\frac{dn}{d\lambda}\right)} \cdot \frac{s}{f} \qquad \text{(A-6)}$$

In the case of a prism used at minimum deviation*,

$$\frac{d\theta}{dn} = \frac{2\sin\left(\frac{\alpha}{2}\right)}{(1-n^2\sin^2(\alpha/2))^{\frac{1}{2}}} \qquad \text{(A-7)}$$

where n is the index of refraction of the prism at wavelength λ and α is the prism apex angle. Therefore

$$(\Delta\lambda)_d = \frac{\left[1-n^2\sin^2(\alpha/2)\right]^{\frac{1}{2}}}{2\sin(\alpha/2)} \cdot \frac{1}{(dn/d\lambda)} \cdot \frac{s}{f} \qquad \text{(A-8)}$$

For a single pass monochromator the radiation passes through the prism two times and both the entrance and exit slits have the same slit width**, the resolved band width due to the dispersion of the prism should be half of the above, i.e.

$$(\Delta\lambda)_d = \frac{\left[1-n^2\sin^2(\alpha/2)\right]^{\frac{1}{2}}}{4\sin(\alpha/2)(dn/d\lambda)} \cdot \frac{s}{f} \qquad \text{(A-9)}$$

---

*When prisms are used in spectrometers, they are always set as nearly as possible at minimum deviation because otherwise any slight divergence or convergence of the incident light would cause astigmatism in the image (33)

**For: (a) The monochromator can be used interchangeably between entrance slit and exit slit.

(b) For a given sum of entrance and exit slits, the errors or corrections due to wide slits are least when the two slits are equal (23).

Determination of $(\Delta\lambda)_p$ - The equation of resolved band width due to diffraction limitation of a prism is well known and is given as (33)

$$(\Delta\lambda)_p = \frac{\lambda}{b(dn/d\lambda)} \qquad \text{(A-10)}$$

where b is the effective prism base. For a single pass monochromator the radiation passes through the prism two times, which will give two times better resolution as mentioned above, i.e.

$$(\Delta\lambda)_p = \frac{\lambda}{2b(dn/d\lambda)} \qquad \text{(A-11)}$$

Actually $(\Delta\lambda)_p$ will depend on the slit width as well (40)

$$(\Delta\lambda)_p = F(s)\ \frac{\lambda}{2b(dn/d\lambda)} \qquad \text{(A-12)}$$

with F(s) a function of slit width. Usually, $(\Delta\lambda)_d$ is much larger than the term $(\Delta\lambda)_p$, thus F(s) is only a second order correction. For simplicity without introducing large error, set F(s)=1, and the equation of $(\Delta\lambda)$ becomes

$$\Delta\lambda = \frac{\left[1-n^2\sin^2(\alpha/2)\right]^{-\frac{1}{2}}}{4\sin(\alpha/2)(dn/d\lambda)} \cdot \frac{s}{f} + \frac{\lambda}{2b(dn/d\lambda)} \qquad \text{(A-13)}$$

for a single pass monochromator. Equation (A-13) can be written as

$$\Delta\lambda = \Delta\lambda_{0.1} \cdot \frac{s}{0.1} + \Delta\lambda_p \qquad \text{(A-14)}$$

where $\Delta\lambda_{0.1}$ is the resolved band width due to dispersion for 0.1 mm slit width and s is the slit width used in the unit of mm.

In Figure 8A of reference (40), $\Delta\lambda_{0.1}$ and $\Delta\lambda_p$ as

functions of wavelength are given for the double pass monochromator. These values should be doubled in order to calculate the resolved band width for a single pass monochromator.

By using values of $\Delta\lambda_{0.1}$ and $\Delta\lambda_{p}$ taken from curves in Figure 8A of reference (40) and using Equation (A-14), the resolved band widths of the P-E Model 98 single pass monochromator are calculated for wavelengths from two to 13 microns and with slit openings from 0.1 mm to 1.6 mm. The results are listed in Table A-1.

Table A-1. Resolved Band Width (in microns) of Single Pass Monochromator

Wavelength	Slit Opening (mm)				
μ	0.1	0.2	0.4	0.8	1.60
2	0.0450	0.0850	0.1650	0.3250	0.6450
3	0.0604	0.1124	0.2164	0.4202	0.8404
4	0.0672	0.1042	0.1982	0.3862	0.7622
5	0.0478	0.0848	0.1588	0.3068	0.6028
6	0.0420	0.0730	0.1350	0.2590	0.5070
7	0.0370	0.0630	0.1150	0.2190	0.4270
8	0.0338	0.0568	0.1028	0.1948	0.3788
9	0.0304	0.0504	0.0904	0.1704	0.3304
10	0.0288	0.0478	0.0858	0.1618	0.3138
11	0.0274	0.0454	0.0804	0.1534	0.2974
12	0.0264	0.0438	0.0786	0.1482	0.2874
13	0.0260	0.0432	0.0786	0.1464	0.2840

APPENDIX C

THEORY CONCERNING FLUX AVERAGING SPHERE

A flux averaging sphere is a sphere with diffusive inner coating and used over the detector (see Figure A-2). The function of the flux averaging sphere is to spread the incident flux uniformly over the sensitive area of the detector, regardless of image size, shape, or intensity distribution. One can thus eliminate the problems of spatial sensitivity, angular sensitivity, and collection of all of the incident flux due to the image over filling the detector which might be caused by aberrations and any slight mis-alignment of the optical components.

Jacquez and Kuppenheim (32) developed the general theory for the performance of an integrating sphere expressed in the relation

$$B_D = P \cdot r_s \frac{b/S}{1 - \left(\frac{r_\omega \, d}{S}\right) - r_s \, c/S} = (Pr_s)\eta \qquad \text{(A-15)}$$

where

B_D is the total flux passing out through the detector port with the sample at the sample aperture.

P is the total radiant incident flux into the entrance port

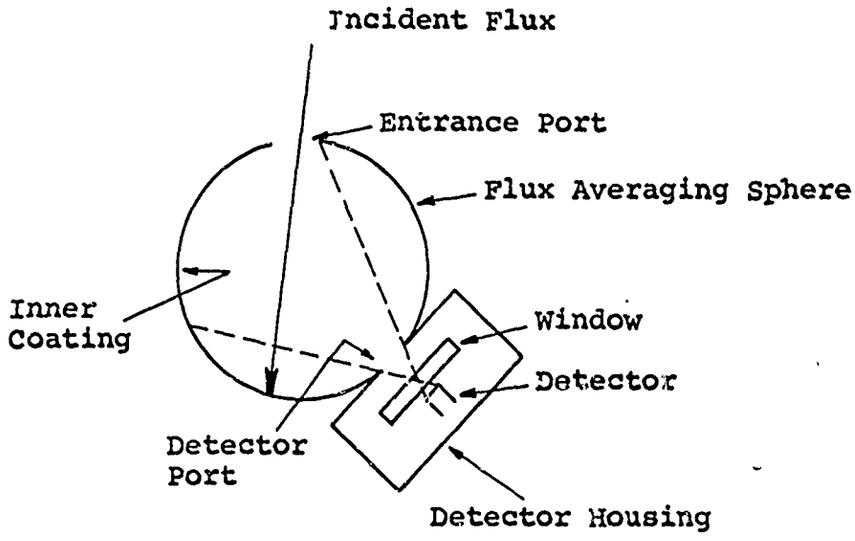

Figure A-2. Sketch of Flux Averaging Sphere.

η is the efficiency of the sphere.

r_s is the reflectance of the sample.

a is the spherical area of entrance port.

b is the spherical area of detector port.

c is the spherical area of sample port.

$S=4\pi R^2$, R is the radius of the sphere.

r_ω is the reflectance of sphere inner coating.

d=S-a-b-c

An averaging sphere has only one entrance port, one detector port, and no sample port, hence the general relation reduces to a simpler form in the case of an "averaging sphere."

$$B_D = P \frac{b/S}{(1/r_\omega)-1 + (a/s) + (b/S)} \qquad \text{(A-16)}$$

For designing a sphere to serve the purpose of flux averaging, the sphere should fulfill the following conditions:

1. The wall of the sphere should be coated with a material which will give high reflectance in the wavelength range concerned.
2. The sphere wall should be a diffusing surface if a constant intensity across the detector port is to be expected.
3. The sphere size should be small.
4. The detector port should be as large as practical .
5. The entrance port should be as small as possible.

Averaging spheres of two and three inch diameters, with Roto-blasting inner surface and sulfur coating (18) were fabricated. Both entrance and detector ports were of the size 5/16 inch x 1/2 inch.

With the above given dimensions, the total flux reaching the detector, B_D, can be estimated theoretically. For simplicity in calculation of B_D, the areas of entrance and detector ports are neglected comparing to the total surface area of the sphere. Thus, the equation of B_D become

$$B_D = P \frac{b/S}{(1/r_\omega)-1} \qquad \text{(A-17)}$$

The reflectance of the coating (sulfur), r_ω, is from 0.95 to 0.75 for the wavelength range from 1.5μ to 7.0μ (18).

The total flux reaching the detector, B_D, is calculated for averaging spheres with two and three inch diameter at wavelengths 1.5μ and 7.0μ. The results of B_D are given in percentages of the incident flux to the entrance port (see Table A-2).

Table A-2. Total Flux Reaching The Detector.

λ (μ)	Total Flux Reaching the Detector	
	3 inch sphere	2 inch sphere
1.5	11.0% P	25.0% P
7.0	1.7% P	3.7% P

Different coating thicknesses and detector port configurations of the averaging spheres were tried. The maximum radiant flux received on the detector was about one-fourth of the value predicted in Table A-2. That is, at about 2μ the radiant flux received on the detector with the averaging sphere is only about 6% of the radiant flux

received on the detector without the averaging sphere and at 7.0μ it is only 0.9%.

VITA

Jack Jim Coe Hsia is a citizen of the Republic of China,

After high school, Mr. Hsia attended National Taiwan University, and received the B.S.M.E. degree in June 1959. Upon receipt of his degree from National Taiwan University, he served as a ground engineer with the rank of second lieutenant in the Chinese Air Force until February 1961.

In September 1961, Mr. Hsia entered Purdue University, where he served as a graduate research assistant at the Thermophysical Properties Research Center and was awarded the M.S.M.E. degree in June 1964. He remained at Purdue University to study towards a doctorate.

Mr. Hsia is a student member of the Optical Society of America and an associate member of the American Society of Mechanical Engineers.

Mr. Hsia and his wife,